Journal of Applied Mathematics and Physics, 2022, 10, 960-999
https://www.scirp.org/journal/jamp
ISSN Online: 2327-4379
ISSN Print: 2327-4352

Simple Proofs of Upper and Lower Envelopes of Van Der Pauw's Equation for Hall-Plates with an Insulated Hole and Four Peripheral Point-Contacts

Udo Ausserlechner

Department of Sense and Control, Infineon Technologies AG, Villach, Austria
Email: udo.ausserlechner@infineon.com

How to cite this paper: Ausserlechner, U. (2022) Simple Proofs of Upper and Lower Envelopes of Van Der Pauw's Equation for Hall-Plates with an Insulated Hole and Four Peripheral Point-Contacts. *Journal of Applied Mathematics and Physics*, **10**, 960-999.
https://doi.org/10.4236/jamp.2022.103066

Received: February 17, 2022
Accepted: March 28, 2022
Published: March 31, 2022

Abstract

For plane singly-connected domains with insulating boundary and four point-sized contacts, $C_0 \cdots C_3$, van der Pauw derived a famous equation relating the two trans-resistances $R_{01,23}, R_{12,30}$ with the sheet resistance without any other parameters. If the domain has one hole van der Pauw's equation becomes an inequality with upper and lower bounds, the envelopes. This was conjectured by Szymański *et al.* in 2013, and only recently it was proven by Miyoshi *et al.* with elaborate mathematical tools. The present article gives new proofs closer to physical intuition and partly with simpler mathematics. It relies heavily on conformal transformation and it expresses for the first time the trans-resistances and the lower envelope in terms of Jacobi functions, elliptic integrals, and the modular lambda elliptic function. New simple formulae for the asymptotic limit of a very large hole are also given.

Keywords

Conformal Mapping, Contraction Process, Doubly Connected Domains, Envelopes, Hall Plate, Large Hole Angle, Sheet Resistance, Small Hole Angle, Van Der Pauw

1. Introduction

The sheet resistance of a plane conductive layer is of prime importance in thin layer technologies. It is used pervasively in micro-electronic manufacturing to monitor the properties of thin conductive layers. It is given by $R_{\text{sheet}} = 1/(\kappa t_{\perp})$, where κ is the conductivity and $t_{\perp}$ is the thickness of the layer. Van der

Pauw showed that it is possible to derive the sheet resistance from purely electrical measurements of currents and voltages, no other geometrical parameters are necessary [1] [2]. Yet some general requirements have to be granted: the conductive layer has to be *plane*, its resistivity and thickness must be *homogeneous*, the contacts must be small (*point-sized*), and the contacts must be on the circumference (=*peripheral* contacts) of a *singly-connected* region (no holes). Homogeneous resistivity also means a linear material law of electric conduction where resistivity is constant versus electric field, without self-heating, and without self-magnetic field. The resistivity is allowed to be anisotropic with a symmetric resistivity tensor. In this case we can apply an isotropization procedure as shown in [3] [4] [5]. At the beginning we rule out anti-symmetric resisitivity tensors as they occur if magnetic fields are applied, but Section 4 extends the range of validity to include the Hall-effect.

The plane conductive region of a conventional Hall-plate has four peripheral point-sized contacts with consecutive labels 0, 1, 2, 3 in a positive mathematical direction (*i.e.* counter-clockwise). Thus, if we move along the boundary from contact 0 via 1 and 2 to 3 (in ascending order) the conductive region is on the left hand side. If current is forced to flow between two contacts and the voltage is tapped between two contacts, then van der Pauw used the ratio

$$R_{k\ell,mn} = \left(V_n - V_m\right) / I_{k\ell} \quad \forall k,\ell,m,n \in \{0,1,2,3\}. \tag{1}$$

V_m, V_n are the electric potentials at the *m*-th and *n*-th contacts, and $I_{k\ell}$ is the current entering the conductive region through contact *k* and leaving it through contact ℓ. The quantity $R_{k\ell,mn}$ has the dimension "voltage over current", which is a resistance. The contacts for the current may be the same or they may be different from the contacts for tapping the voltage, in the latter case we call $R_{k\ell,mn}$ a trans-resistance. Depending on the sequence of the indices, trans-resistances may be positive or negative. Van der Pauw chose the sign in the definition (1) such that for rising sequence of contacts and their cyclic permutations the trans-resistances are positive, $R_{01,23} > 0, R_{12,30} > 0$. For point-sized contacts, the *trans*-resistances are the only finite resistances.

For the sake of brevity, I define *van der Pauw's function*

$$\mathrm{vdP} := \underbrace{\exp\left(-\pi R_{01,23}/R_{\text{sheet}}\right)}_{:=X} + \underbrace{\exp\left(-\pi R_{12,30}/R_{\text{sheet}}\right)}_{:=Y}. \tag{2}$$

X and *Y* are abbreviations for the exponential terms. Then the basic result for Hall-plates without a hole in [1] is *van der Pauw's equation*,

$$\mathrm{vdP} = 1. \tag{3}$$

In the *van der Pauw plane* (X,Y) Equation (3) is a straight line $Y = 1 - X$. The peculiarity of (3) lies in the fact that it relates measurable electrical quantities $R_{01,23}, R_{12,30}$ to the sheet resistance R_{sheet} irrespective of any geometrical details, neither the shape of the Hall-plate nor the locations of the contacts are specified. Having measured the two trans-resistances, one can solve the nonlinear Equation (3) to get the sheet resistance. This is van der Pauw's method to determine the sheet resistance. It works well in many practical cases.

However, occasionally one faces the problem that some of the above given requirements are not fullfilled. Then van der Pauw's method gives inaccurate or even wrong results for the sheet resistance. This is an inherent problem in materials science, where one needs to characterize novel materials. Often these samples have poor quality and poor homogeneity due to limitations in the manufacturing process, especially when the fabrication on a small laboratory scale is not yet mature [6] [7] [8]. From a practical standpoint, one would like to have a procedure that detects poor sample homogeneity and that gives error bounds for the derived sheet resistance. Inhomogeneous conductivity is supposed to have a similar effect to small voids. This is the motivation to study Hall-plates with holes.

The topic was pioneered over the last decade in a couple of papers by Szymański and coworkers [9] [10] [11] [12]. They introduced the concept of upper and lower envelopes (u.e., l.e.) for conductive samples with a hole,

$$\text{l.e.} \le \text{vdP} \le \text{u.e.} = 1. \tag{4}$$

For constant hole size, the lower envelope depends only on X. Further contributions came from [13]. For nearly one decade (4) was just a conjecture, while a strict mathematical proof was missing, until only recently a thesis solved this problem (with its potential generalization to more than one hole) at a fairly elaborate mathematical level [14] [15]. The present article gives new and simpler proofs for samples with a single hole with less sophisticated mathematics and closer to the physical intuition of an electrical engineer. The employed mathematical tools are series expansions and conformal transformations which lead to Jacobi functions and elliptic integrals.

There is a certain similarity of the current topic with another topic called the Hall/Anti-Hall bar [16] [17]. No Hall voltage appears there between any two points on the hole boundary if current flows between two points on the outer boundary of the Hall-plate. In van der Pauw's measurement current flows between neighboring contacts and voltages are also tapped between neighboring contacts, whereas in common Hall-plates current flows between non-neighboring contacts and voltages are tapped between other non-neighboring contacts. In the Hall/Anti-Hall bar we cannot speak of neighboring contacts anymore, because current and voltage contacts are on different boundaries. The focus of interest in the Hall/Anti-Hall bar lies on the case of applied magnetic field (*i.e.*, the Hall-effect with non-reciprocal conductivity tensor), whereas the focus of the present article lies on the case of zero magnetic field (*i.e.*, simple ohmic conduction with scalar conductivity).

This article starts with the easier case of a small hole, which leads us straight to the star-configuration and the minimum of the van der Pauw function. Then we compute the trans-resistances for arbitrary hole size with conformal transformations, and we prove the upper and lower envelopes. We discuss some properties of the trans-resistances and how they are affected by a magnetic field.

Finally, we check the derived formulae with numerical simulations.

2. Hall-Plates with a Small Hole

2.1. Series Expansion of the Potential

Let us start with a plane irregular ideal Hall-plate with a single irregular hole of arbitrary size. The entire inner and outer boundary is insulating except for four point-sized contacts $C_0,\cdots,C_3$. Current I_{01} is injected by an ideal current source at C_0 and extracted at C_1 while the voltage from C_3 to C_2 is measured. We know from Riemann that a conformal map exists, which maps the irregular Hall-plate onto the unit disk with a central hole of radius $0<r_1<1$, whereby r_1 is the Riemann modulus of the singly-connected domain. Let us rotate the disk such that the current contacts C_0,C_1 are symmetrical to the real axis. Then, the azimuthal locations of the contacts are (see **Figure 1**)

$$\varphi(C_0)=2\pi-\varphi_1,\quad \varphi(C_1)=\varphi_1,\quad \varphi(C_2)=\varphi_2,\quad \varphi(C_3)=\varphi_3, \tag{5}$$

with $0<\varphi(C_\ell)<2\pi$ being the azimuthal angle of the location of C_ℓ. The electrostatic potential at zero magnetic field, ϕ_0, is given in [17]. At the outer perimeter, it holds

$$\phi_0=I_{01}R_{\text{sheet}}\frac{-2}{\pi}\sum_{\ell=1}^{\infty}\frac{1+r_1^{2\ell}}{1-r_1^{2\ell}}\sin(\ell\varphi_1)\frac{\sin(\ell\varphi)}{\ell}. \tag{6}$$

(6) is derived from a Fourier series which solves the Laplace equation of the potential in the annular region with insulating boundary conditions at the perimeter and at the hole. With $r_1^{2\ell}=q$ and

$$\frac{1+q}{1-q}=1+\frac{2q}{1-q}=1+2\sum_{m=1}^{\infty}q^m \tag{7}$$

(see (102) in Appendix A) this is

$$\phi_0=I_{01}R_{\text{sheet}}\frac{-2}{\pi}\sum_{\ell=1}^{\infty}\left(1+2\sum_{m=1}^{\infty}r_1^{2m\ell}\right)\sin(\ell\varphi_1)\frac{\sin(\ell\varphi)}{\ell}. \tag{8}$$

With (105) we get

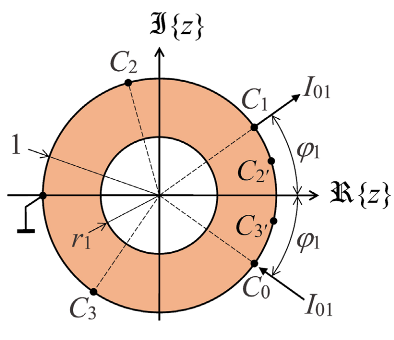

Figure 1. Plane annular Hall-plate with insulating boundaries and point-sized peripheral contacts $C_0\cdots C_3$. Current flows from C_0 to C_1. Voltage is tapped between C_3 and C_2. The potentials in $C_{2'},C_{3'}$ are identical to the potentials in C_2,C_3, respectively (see Section 3.2).

$$\begin{aligned}\phi_0 &= I_{01} R_{\text{sheet}} \frac{1}{2\pi} \ln\left(\frac{1-\cos(\varphi-\varphi_1)}{1-\cos(\varphi+\varphi_1)} \right) \\ &+ I_{01} R_{\text{sheet}} \frac{-2}{\pi} 2 \sum_{\ell=1}^{\infty} \frac{1}{4} \ln\left(\frac{1+r_1^{4\ell} - 2r_1^{2\ell}\cos(\varphi+\varphi_1)}{1+r_1^{4\ell} - 2r_1^{2\ell}\cos(\varphi-\varphi_1)} \right).\end{aligned} \tag{9}$$

Rearranging this gives

$$\frac{\phi_0}{I_{01}} = \frac{R_{\text{sheet}}}{\pi} \ln\left(\sqrt{\frac{1-\cos(\varphi-\varphi_1)}{1-\cos(\varphi+\varphi_1)}} \prod_{\ell=1}^{\infty} \frac{1+r_1^{4\ell} - 2r_1^{2\ell}\cos(\varphi-\varphi_1)}{1+r_1^{4\ell} - 2r_1^{2\ell}\cos(\varphi+\varphi_1)} \right), \tag{10}$$

which is equivalent to

$$\exp\left(\frac{2\pi\phi_0}{R_{\text{sheet}} I_{01}} \right) = \prod_{\ell=-\infty}^{\infty} \frac{\left(\cosh(\ell \ln(r_1))\right)^2 - \left(\cos\left(\frac{\varphi-\varphi_1}{2}\right)\right)^2}{\left(\cosh(\ell \ln(r_1))\right)^2 - \left(\cos\left(\frac{\varphi+\varphi_1}{2}\right)\right)^2}. \tag{11}$$

The term $\ell = 0$ corresponds to the singly-connected Hall region with $r_1 = 0$. The measured van-der-Pauw voltage is $V_{32} = \phi_0(\varphi_3) - \phi_0(\varphi_2)$. With $R_{01,23} = V_{32}/I_{01}$ this gives

$$\begin{aligned}X = \exp\left(\frac{-\pi R_{01,23}}{R_{\text{sheet}}} \right) = \prod_{\ell=-\infty}^{\infty} \Bigg[&\frac{\left(\cosh(\ell \ln(r_1))\right)^2 - \left(\cos\left(\frac{\varphi_2-\varphi_1}{2}\right)\right)^2}{\left(\cosh(\ell \ln(r_1))\right)^2 - \left(\cos\left(\frac{\varphi_2+\varphi_1}{2}\right)\right)^2} \\ &\times \frac{\left(\cosh(\ell \ln(r_1))\right)^2 - \left(\cos\left(\frac{\varphi_3+\varphi_1}{2}\right)\right)^2}{\left(\cosh(\ell \ln(r_1))\right)^2 - \left(\cos\left(\frac{\varphi_3-\varphi_1}{2}\right)\right)^2} \Bigg]^{1/2}.\end{aligned} \tag{12}$$

If we inject the current at C_1, extract it at C_2 and measure $V_{03} = \phi_0(\varphi_0) - \phi_0(\varphi_3)$ we can re-use (12) if we replace

$$\begin{aligned}\varphi_1 &\mapsto \frac{\varphi_2-\varphi_1}{2} \\ \varphi_2 &\mapsto (\varphi_3-\varphi_2) + \frac{\varphi_2-\varphi_1}{2} = \varphi_3 - \frac{\varphi_2+\varphi_1}{2} \\ \varphi_3 &\mapsto (2\pi-\varphi_1-\varphi_3) + (\varphi_3-\varphi_2) + \frac{\varphi_2-\varphi_1}{2} = 2\pi - \frac{3\varphi_1+\varphi_2}{2}.\end{aligned} \tag{13}$$

With $R_{12,30} = V_{03}/I_{12}$ this gives

$$\begin{aligned}Y = \exp\left(\frac{-\pi R_{12,30}}{R_{\text{sheet}}} \right) = \prod_{\ell-\infty}^{\infty} \Bigg[&\frac{\left(\cosh(\ell \ln(r_1))\right)^2 - \left(\cos\left(\frac{\varphi_3-\varphi_2}{2}\right)\right)^2}{\left(\cosh(\ell \ln(r_1))\right)^2 - \left(\cos\left(\frac{\varphi_2+\varphi_1}{2}\right)\right)^2} \\ &\times \frac{\left(\cosh(\ell \ln(r_1))\right)^2 - \left(\cos(\varphi_1)\right)^2}{\left(\cosh(\ell \ln(r_1))\right)^2 - \left(\cos\left(\frac{\varphi_3-\varphi_1}{2}\right)\right)^2} \Bigg]^{1/2}.\end{aligned} \tag{14}$$

A Taylor series for *small holes* $r_1 \ll 1$ keeps only the terms $\ell = -1, 0, 1$,

$$X = X_0 + \mathrm{d}X_0 r_1^2 + \mathcal{O}(r_1)^4, \quad Y = Y_0 + \mathrm{d}Y_0 r_1^2 + \mathcal{O}(r_1)^4, \tag{15}$$

with

$$\begin{aligned}
X_0 &= \frac{\cos((\varphi_2+\varphi_3)/2) - \cos(\varphi_1 + (\varphi_3-\varphi_2)/2)}{\cos((\varphi_2+\varphi_3)/2) - \cos(\varphi_1 - (\varphi_3-\varphi_2)/2)},\\
Y_0 &= 1 - X_0,\\
\mathrm{d}X_0 &= 4X_0 \cos\left(\frac{\varphi_2+\varphi_3}{2}\right)\left(\cos\left(\varphi_1 - \frac{\varphi_3-\varphi_2}{2}\right) - \cos\left(\varphi_1 + \frac{\varphi_3-\varphi_2}{2}\right)\right),\\
\mathrm{d}Y_0 &= 4Y_0 \cos\left(\varphi_1 - \frac{\varphi_3-\varphi_2}{2}\right)\left(\cos\left(\frac{\varphi_2+\varphi_3}{2}\right) - \cos\left(\varphi_1 + \frac{\varphi_3-\varphi_2}{2}\right)\right).
\end{aligned} \tag{16}$$

X, Y are defined in (2), X_0, Y_0 are the values for $r_1 = 0$, and $\mathrm{d}X_0, \mathrm{d}Y_0$ are the lowest order terms in r_1.

$$\begin{aligned}
\mathrm{vdP} &= X + Y\\
&= 1 - r_1^2 \times 16 \sin(\varphi_1) \sin\left(\frac{\varphi_2-\varphi_1}{2}\right) \sin\left(\frac{\varphi_3-\varphi_2}{2}\right) \sin\left(\frac{\varphi_3+\varphi_1}{2}\right) + \mathcal{O}(r_1)^4\\
&< 1.
\end{aligned} \tag{17}$$

In this equation, the coefficient of r_1^2 is positive, because $0 < \varphi_1 < \pi$ and $\varphi_1 < \varphi_2 < \varphi_3 < 2\pi - \varphi_1$. This is the simple proof that a small *insulating* hole *reduces* the van der Pauw function below 1. Equation (17) is also derived in [9].

2.2. Derivation of the Star-Configuration of Contacts

A general contact arrangement is defined by three parameters $\varphi_1, \varphi_2, \varphi_3$. For a specific set $(\varphi_1, \varphi_2, \varphi_3)$ a certain value for $Y_0 = 1 - X_0$ follows. Yet, according to (16) there are many other sets $(\varphi_1, \varphi_2, \varphi_3)$ which give the same X_0, Y_0. Which of all these sets causes the steepest drop of vdP for small holes? In other words, for fixed trans-resistances of a singly-connected Hall-plate, how do we have to place the contacts such that the van der Pauw function becomes most sensitive to a small nucleating hole? Keeping X_0 fixed implicitly defines the azimuthal position φ_1 as a funcion of the other two positions, $\varphi_1 = \varphi_1(\varphi_2, \varphi_3)$. From $X_0 = const$ it follows $\partial X_0 / \partial\varphi_2 = 0$ and $\partial X_0 / \partial\varphi_3 = 0$, which gives

$$\frac{\partial X_0}{\partial\varphi_1}\frac{\partial\varphi_1}{\partial\varphi_2} + \frac{\partial X_0}{\partial\varphi_2} = 0, \quad \frac{\partial X_0}{\partial\varphi_1}\frac{\partial\varphi_1}{\partial\varphi_3} + \frac{\partial X_0}{\partial\varphi_3} = 0. \tag{18}$$

The minimum of $\mathrm{d}X_0 + \mathrm{d}Y_0$ means the largest negative slope of vdP versus r_1^2 for $r_1 \to 0$. There it holds $\partial(\mathrm{d}X_0 + \mathrm{d}Y_0)/\partial\varphi_2 = 0$ and $\partial(\mathrm{d}X_0 + \mathrm{d}Y_0)/\partial\varphi_3 = 0$, which gives

$$\begin{aligned}
\frac{\partial(\mathrm{d}X_0 + \mathrm{d}Y_0)}{\partial\varphi_1}\frac{\partial\varphi_1}{\partial\varphi_2} + \frac{\partial(\mathrm{d}X_0 + \mathrm{d}Y_0)}{\partial\varphi_2} &= 0,\\
\frac{\partial(\mathrm{d}X_0 + \mathrm{d}Y_0)}{\partial\varphi_1}\frac{\partial\varphi_1}{\partial\varphi_3} + \frac{\partial(\mathrm{d}X_0 + \mathrm{d}Y_0)}{\partial\varphi_3} &= 0.
\end{aligned} \tag{19}$$

We solve (18) for $\partial\varphi_1/\partial\varphi_2$ and $\partial\varphi_1/\partial\varphi_3$ and insert this into (19). With (16) and after some manipulation this gives

$$\cos(2\varphi_1)=\cos(\varphi_2-\varphi_3)\wedge\cos(\varphi_1)\left(\cos(\varphi_2)-\cos(\varphi_3)\right)=0, \tag{20}$$

with the only meaningful solution

$$\varphi_2^\star=\pi-\varphi_1^\star \quad\wedge\quad \varphi_3^\star=\pi+\varphi_1^\star. \tag{21}$$

Let us call this specific pattern of contacts a *star-configuration*—the contacts are in the vertices of a *rectangle* inscribed into the perimeter of the Hall-plate.

For fixed trans-resistances $R_{01,23}$ and $R_{12,30}$ the drop in the van der Pauw function caused by a small hole gets largest, if the contacts are in a star-configuration.

Inserting (21) into (17) gives

$$\mathrm{vdP}^\star=1-4r_1^2\left(\sin\left(2\varphi_1^\star\right)\right)^2+\mathcal{O}(r_1)^4. \tag{22}$$

From all star-configurations the one with the steepest decline of vdP versus r_1^2 is for

$$\varphi_1^\star=\frac{\pi}{4},\quad \varphi_2^\star=\frac{3\pi}{4},\quad \varphi_3^\star=\frac{5\pi}{4}, \tag{23}$$

where all four contacts are equidistant, *i.e.*, they are in the vertices of a *square* inscribed in the perimeter of the Hall-plate. This configuration gives the smallest possible vdP for a given hole of small size r_1,

$$\mathrm{vdP}_{\min}=1-4r_1^2+8r_1^4-16r_1^6+32r_1^8-56r_1^{10}+96r_1^{12}+\mathcal{O}(r_1)^{14}. \tag{24}$$

Inserting (21) into (16) into (15) gives

$$\begin{aligned}X^\star&=\left(1-8r_1^2\sin^2\left(\varphi_1^\star\right)\right)\cos^2\left(\varphi_1^\star\right)+\mathcal{O}(r_1)^4,\\ Y^\star&=\left(1-8r_1^2\cos^2\left(\varphi_1^\star\right)\right)\sin^2\left(\varphi_1^\star\right)+\mathcal{O}(r_1)^4.\end{aligned} \tag{25}$$

Eliminating $\varphi_1^\star$ from (25) gives a curve in the van der Pauw plane (X,Y), which holds for star-configurations with small holes, $r_1\ll 1/\sqrt{8}$,

$$Y^\star=\frac{1}{8r_1^2}\left(1+8r_1^2X^\star-\sqrt{\left(1-8r_1^2\right)^2+32r_1^2X^\star}\right). \tag{26}$$

This is the small-hole approximation of the lower envelope as it will be explained in Section 3.3.

For holes of arbitrary size a strict proof of $\mathrm{vdP}\le 1$ appears to be difficult, because the trans-resistance $R_{01,23}$ may *in*crease or *de*crease versus hole radius r_1 for holes of small and moderate size.

Example: For the Hall-plate in **Figure 1** set $\varphi_1=10^\circ$, $\varphi_2=20^\circ$. Then V_{32} (and consequently $R_{01,23}$) *in*creases for $\varphi_3=270^\circ$ while it *de*creases for $\varphi_3=90^\circ$ when the hole grows from $r_1=0\to 0.1\to 0.5$ (see also curves 1, 4 in **Figure 9(a)**).

The decrease of $R_{01,23}$ may come a bit surprizingly: a trans-resistance may get smaller if one cuts out a bigger hole of the conductive medium. For the explanation we consider an elongated asymmetric hole in radial direction extending from the center of the disk up to very close to the perimeter, see **Figure 2**. This asymmetric geometry can be mapped onto a symmetric one with a central circular hole (Any plane domain with a single hole can be mapped conformally to a circular ring with inner radius r_1 and outer radius 1 [18]). The radial slit may be placed in-between the two voltage taps. This increases the trans-resistance. However, it may also be placed outside the two voltage taps. Then, a larger fraction of the total supply voltage drops outside the voltage taps, and therefore the trans-resistance becomes smaller. Thus, by the placement of the hole one can make the voltage V_{32} smaller or larger.

Next we have a look at the trans-resistances of Hall-plates with contacts in a star-symmetry as defined in (21) and shown in **Figure 3(a)**. Without loss of generality, the restriction $\varphi_1 \in (0, \pi/2]$ is used, if $\varphi_1 > \pi/2$ we only have to shift the indices of all contacts by one instance further to pull φ_1 again inside $(0, \pi/2]$. From (12) and (14) we get

$$\begin{aligned} \frac{R^\star_{01,23}}{R^\star_{\text{sheet}}} &= \frac{-2}{\pi} \ln\left(\cos\left(\varphi_1^\star\right) \prod_{\ell=1}^{\infty} \left[1 - \left(\frac{2 r_1^{\star\ell} \sin\left(\varphi_1^\star\right)}{1 + r_1^{\star 2\ell}} \right)^2 \right] \right) \\ \frac{R^\star_{12,30}}{R^\star_{\text{sheet}}} &= \frac{-2}{\pi} \ln\left(\sin\left(\varphi_1^\star\right) \prod_{\ell=1}^{\infty} \left[1 - \left(\frac{2 r_1^{\star\ell} \cos\left(\varphi_1^\star\right)}{1 + r_1^{\star 2\ell}} \right)^2 \right] \right). \end{aligned} \tag{27}$$

In contrast to the example given above, *both* trans-resistances *in*crease with growing hole if the contacts are in a star-configuration. This can be readily seen in (27). The plot in **Figure 3(b)** visualizes this fact. The inequality (17) holds for small holes, and according to (27) both trans-resistances increase for larger holes. Therefore the inequality $\text{vdP} \le 1$ holds also for large holes in the case of a $\star$-symmetry.

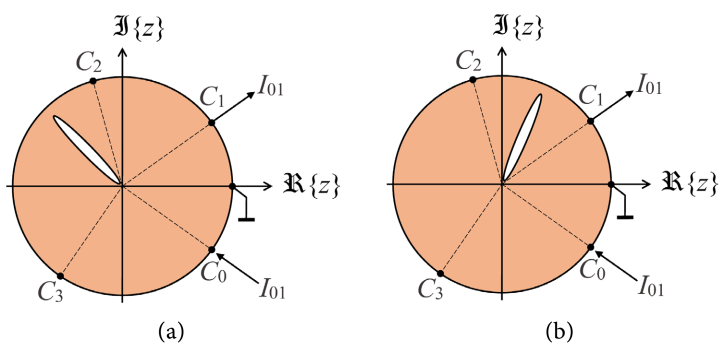

Figure 2. A radial slit may *in*crease or *de*crease a trans-resistance depending on its location. Yet, if it increases the first trans-resistance $R_{01,23}$, it decreases the second trans-resistance $R_{12,30}$. (a) Circular Hall-plate with a radial slit between the voltage taps $C_3 - C_2$ *in*creases $R_{01,23}$ when the hole grows; (b) Circular Hall-plate with a radial slit outside the voltage taps $C_3 - C_2$ *de*creases $R_{01,23}$ when the hole grows.

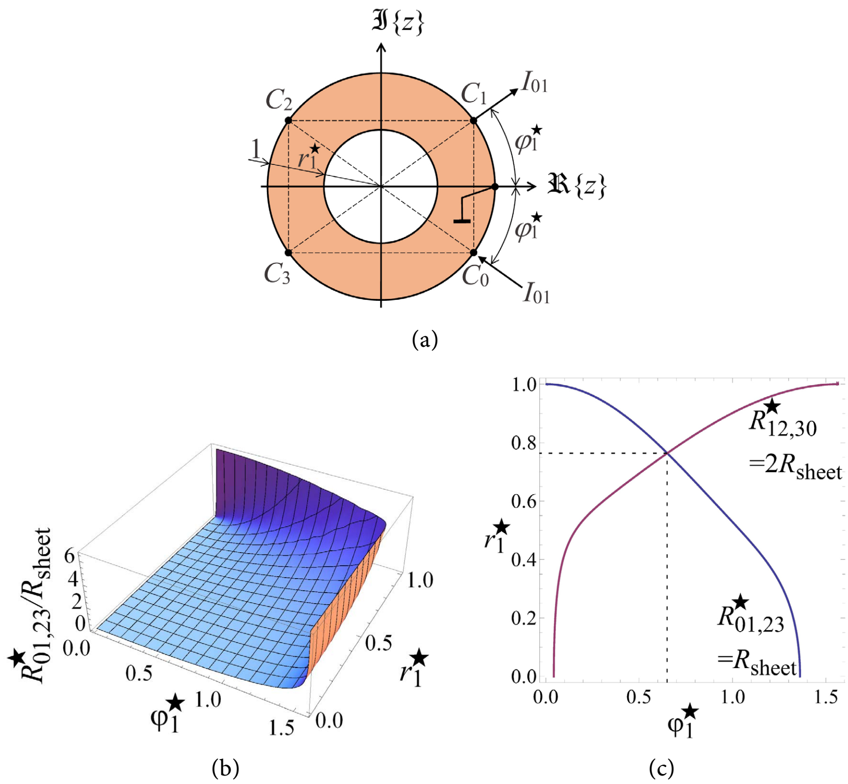

Figure 3. A symmetrical annular Hall-plate with four symmetrical point contacts has three degrees of freedom, $\varphi_1^\star$, $r_1^\star$, and R_{sheet}. Its transresistance $R_{01,23}^\star$ is a concave surface above the $\left(\varphi_1^\star, r_1^\star\right)$-plane. Two values of trans-resistances, $R_{01,23}^\star = R_{\text{sheet}}$ and $R_{12,30}^\star = 2 \times R_{\text{sheet}}$, give two curves in the $\left(\varphi_1^\star, r_1^\star\right)$-plane, which intersect in a unique point $\left(\varphi_1^\star, r_1^\star\right) = \left(0.650645, 0.763757\right)$. (a) A symmetric annular Hall-plate (⋆) with four point-contacts in the vertices of an inscribed rectangle; (b) Its normalized trans-resistance $R_{01,23}^\star / R_{\text{sheet}}$ versus $\varphi_1^\star$ and $r_1^\star$ is a concave surface subtending all values $0 < R_{01,23}^\star < \infty$; (c) Two intersecting curves are generated, when the surfaces $R_{01,23}^\star$ and $R_{12,30}^\star$ are cut through at different heights R_{sheet} and $2 \times R_{\text{sheet}}$.

The two functions in (27) have a couple of useful properties. Not only are they monotonic in $r_1^\star$, they are also monotonic in $\varphi_1^\star$ in the relevant interval $0 \le \varphi_1^\star \le \pi/2$. $R_{01,23}^\star$ strictly increases with $\varphi_1^\star$, whereas $R_{12,30}^\star$ strictly decreases. Both functions are mirrored at $\varphi_1^\star = \pi/4$ (note that the terms $\sin\left(\varphi_1^\star\right)$ and $\cos\left(\varphi_1^\star\right)$ are swapped in the two equations in (27)). For a fixed value of $r_1^\star$ the trans-resistance $R_{01,23}^\star$ goes from $0 \to \infty$ if $\varphi_1^\star$ goes from $0 \to 90^\circ$. Conversely, $R_{01,23}^\star$ goes from $(2/\pi) R_{\text{sheet}} \left|\ln\left(\cos\left(\varphi_1^\star\right)\right)\right| \to \infty$ if $r_1^\star$ goes from $0 \to 1$. Hence, $R_{01,23}^\star$ goes up monotonically if one moves radially away from the origin in the $\left(\varphi_1^\star, r_1^\star\right)$-plane. The surface in **Figure 3(b)** is concave. If the left hand sides in (27) are given, each of the two equations gives a curve in the $\left(\varphi_1^\star, r_1^\star\right)$-plane in the domain $0 \le \varphi_1^\star \le \pi/2, 0 \le r_1^\star \le 1$. The first curve encircles the origin while the second curve encircles the point $\left(\varphi_1^\star, r_1^\star\right) = \left(\pi/2, 0\right)$ (because of the mirror symmetry of both surfaces, see also **Figure 3(c)**). Each curve gives $r_1^\star$ as a strictly monotonic function of $\varphi_1^\star$. If we intersect the $R_{01,23}^\star$-surface at two different heights we get two curves, which have no common point (they do not intersect and they do not touch). If we mirror the second curve at $\varphi_1^\star = \pi/4$ this reflects the measurement of the second trans-resistance $R_{12,30}$. If the two curves cross, due to their monotonicity they have to cross in a single uniquely defined point, which gives $r_1^\star$ and $\varphi_1^\star$ as shown in the example of **Figure 3(c)**. However, if both trans-resistances are very small this would shift the $R_{01,23}$-curve *left* of $\varphi_1^\star = \pi/4$ and the $R_{12,30}$-curve *right* of $\varphi_1^\star = \pi/4$, such that the two curves would not cross at all. In this case the $R_{01,23}$-curve starts at φ_1' at $r_1^\star = 0$ in **Figure 3(c)** while the $R_{12,30}$-curve starts at $\varphi_1'' > \varphi_1'$. With (27) it follows

$$\mathrm{vdP} = X + Y = \underbrace{\cos^2(\varphi_1')}_{=1-\sin^2(\varphi_1')} + \sin^2(\varphi_1'') > 1, \tag{28}$$

because it holds $\sin(\varphi_1') < \sin(\varphi_1'')$ for $0 < \varphi_1' < \varphi_1'' < \pi/2$. Equation (28) contradicts the classical van der Pauw Equation (3) for singly-connected plates ($r_1^\star \to 0$), and therefore we can rule out this case. Thus, we have proven that…

…for any $\star$-arrangement of contacts with fixed sheet resistance the measurement of both trans-resistances $R_{01,23}, R_{12,30}$ defines two curves like in **Figure 3(c)**, which intersect in exactly one point. This point specifies the hole radius $r_1^\star$ and the locations $\varphi_1^\star$ of the contacts.

For any doubly-connected Hall-plate with arbitrary $\varphi_1, \varphi_2, \varphi_3, r_1, R_{\mathrm{sheet}}$ we can find a $\star$-configuration of contacts with $\varphi_1^\star \le \pi/4$, which has the same trans-resistances $R_{01,23} = R_{01,23}^\star, R_{12,30} = R_{12,30}^\star$, but generally different hole size $r_1^\star$ and different sheet resistance $R_{\mathrm{sheet}}^\star$.

The proof goes like this:

Suppose we have a general asymmetrical contact placement, which gives two measurement results $0 \le R_{01,23} \le R_{12,30} < \infty$. If accidentally the measurement returns $R_{01,23} > R_{12,30}$ we simply swap the two trans-resistances by moving all contacts one instance further. Now we consider a hypothetical Hall-plate with a $\star$-symmetry as in **Figure 3(a)**. We choose its sheet resistance

$$R_{\mathrm{sheet}}^\star = \frac{\pi}{\ln(2)} R_{01,23}. \tag{29}$$

Then it follows from (27) that $\varphi_1^\star = \pi/4$, if this Hall-plate had no hole, $r_1^\star = 0$. If it has a hole, $\varphi_1^\star$ is smaller, but at this moment we do not know anything about the hole. If we set $R_{01,23}^\star = R_{01,23}$ we get a first curve in the $(\varphi_1^\star, r_1^\star)$-plane which starts at $(\varphi_1^\star, r_1^\star) = (\pi/4, 0)$ and encircles the origin counter-clockwise. We also set $R_{12,30}^\star = R_{12,30}$, which gives a second curve that encircles the point $(\pi/2, 0)$ in the $(\varphi_1^\star, r_1^\star)$-plane clock-wise. Since $R_{12,30} \ge R_{01,23}$ the second curve starts at a point on the $\varphi_1^\star$-axis, which is left of $\varphi_1^\star = \pi/4$. Therefore, the two curves *must* intersect. Since all curves are strictly monotonic in $\varphi_1^\star$, they must intersect in a single point only. This gives the unique solution of a hypothetical $\star$-Hall-plate, which has the same trans-resistances as our original Hall-plate, albeit it has a different hole and a different sheet resistance.

This argument clearly shows that one cannot determine the sheet resistance of a doubly-connected Hall-plate with the measurement of both trans-resistances as in the singly-connected case, unless one has additional information about the hole or the contacts placements. In general it holds $R_{\text{sheet}}^\star \neq R_{\text{sheet}}$, either one can be larger than the other one. For the $\star$-case the value of the van der Pauw function vdP is bounded: we insert (29) into (2)

$$\text{vdP} = \frac{1}{2} + \exp\left(\frac{-R_{12,30}}{R_{01,23}} \ln(2)\right) = \frac{1}{2} + \left(\frac{1}{2}\right)^{\frac{R_{12,30}}{R_{01,23}}} \leq 1, \tag{30}$$

which is fulfilled due to our assumption $R_{01,23} \leq R_{12,30}$.

3. Hall-Plates with a Large Hole

3.1. Conformal Mapping of the Annular Hall-Plate

Next we apply conformal mapping to the general ring-shaped Hall-plate from Figure 1. Since the current contacts are symmetric to the real axis it is clear that all points $-1 \leq \Re\{z\} \leq -r_1$ and $r_1 \leq \Re\{z\} \leq 1$ on the real axis are at the same potential, say 0 V. There we can insert a contact. We can further cut the ring apart at the positive real axis, apply contacts at both cut edges, and short them with a wire (see Figure 4(a)), without affecting the potential in the annular region. From the discussion in [17] we know that the fraction $(1-\varphi_1/\pi)$ of the current flows through the shorted wire, independent of the size of the hole. The conformal transformation

$$w = \log(z) \tag{31}$$

maps the annulus in the *z*-plane to the rectangle in the *w*-plane shown in Figure 4(b). The width of this rectangle is $|\ln(r_1)|$ and its height is 2π. The outer perimeter of the ring in the *z*-plane appears at the right edge of the rectangle in the *w*-plane, whereas the hole boundary appears at the left side of the rectangle. A Schwartz-Christoffel transformation maps this rectangle from the *w*-plane onto the upper half of the ζ-plane in Figure 4(c),

$$w = c_1 \int \frac{\mathrm{d}\zeta}{\sqrt{\zeta-\zeta_4}\sqrt{\zeta-1}\sqrt{\zeta+1}\sqrt{\zeta+\zeta_4}} + c_2. \tag{32}$$

In the *w*-plane the current contacts C, G are placed symmetrically to the large contacts $\overline{AB}, \overline{HJ}$. Thus, also in the ζ-plane they are symmetrically to the large contacts. From the sequential order of the points on the rectangular boundary in the *w*-plane it follows the same order in the ζ-plane,

$$-\zeta_0 < \zeta_2 < \zeta_3 < \zeta_0 < \zeta_4 < 1 < \zeta_5 \quad \text{with } \zeta_0 > 0. \tag{33}$$

It holds

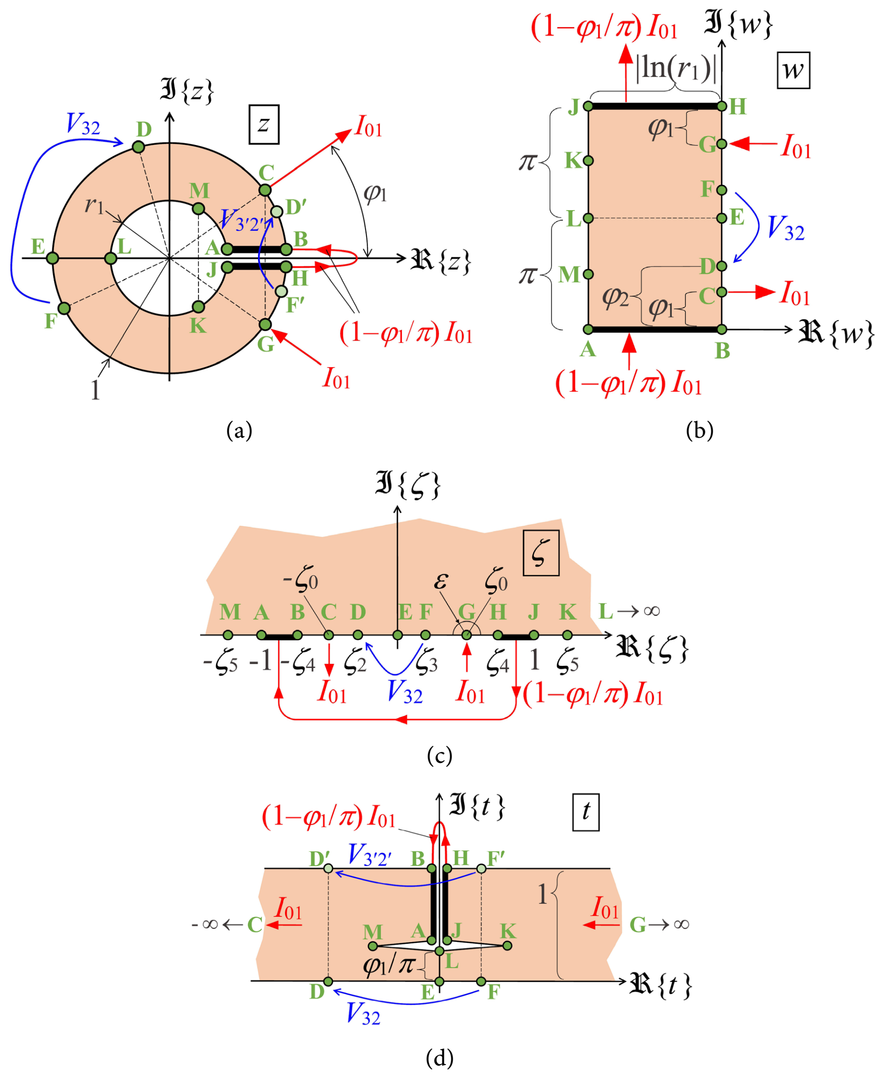

Figure 4. Conformal transformations of a doubly-connected Hall-plate, which is cut open to give a singly-connected Hall-plate if current flows between points G and C. Contacts $\overline{AB} = \overline{HJ}$ are inserted at the cuts. The annular region in the *z*-plane is mapped to a rectangle in the *w*-plane, to the upper half of the ζ-plane and to an infinitely long stripe with a longitudinal slit in the *t*-plane. Points K, M are the stagnation points when current flows between G to C. (a) Hall-plate in the *z*-plane; (b) Hall-plate in the *w*-plane; (c) Hall-plate in the ζ-plane; (d) Hall-plate in the *t*-plane.

$$\left|\ln\left(r_1\right)\right| = w_H - w_J = c_1 \int_1^{\zeta_4} \frac{\mathrm{d}\zeta}{\sqrt{\zeta-\zeta_4}\sqrt{\zeta-1}\sqrt{\zeta+1}\sqrt{\zeta+\zeta_4}} = \frac{-c_1}{i} K'\left(\zeta_4\right), \quad (34)$$

where w_H, w_J are the locations of the points H, J in the *w*-plane, respectively, K' is the complementary complete elliptic integral of the first kind (see Appendix B), and $i = \sqrt{-1}$. It also holds

$$\pi i = w_H - w_E = c_1 \int_0^{\zeta_4} \frac{\mathrm{d}\zeta}{\sqrt{\zeta-\zeta_4}\sqrt{\zeta-1}\sqrt{\zeta+1}\sqrt{\zeta+\zeta_4}} = -c_1 K\left(\zeta_4\right). \quad (35)$$

Combining (34) and (35) gives

$$\frac{|\ln(r_1)|}{\pi}=\frac{K'(\zeta_4)}{K(\zeta_4)} \quad\Rightarrow\quad \zeta_4=\sqrt{L\left(\frac{|\ln(r_1)|}{\pi}\right)}, \tag{36}$$

with the modular lambda elliptic function $L(y)$ (see Appendix B). Inserting the right side of (36) into (35) gives the scaling constant c_1 of the mapping (32). The locations $\pm\zeta_0$ of the point current contacts C,G in the ζ-plane follow from

$$\begin{aligned} i(\pi-\varphi_1) &= w_G-w_E=c_1\int_0^{\zeta_0}\frac{\mathrm{d}\zeta}{\sqrt{\zeta-\zeta_4}\sqrt{\zeta-1}\sqrt{\zeta+1}\sqrt{\zeta+\zeta_4}} \\ &= -c_1F\left(\frac{\zeta_0}{\zeta_4},\zeta_4\right) \quad\Rightarrow\quad \frac{\zeta_0}{\zeta_4}=\mathrm{sn}\left(\left(1-\frac{\varphi_1}{\pi}\right)K(\zeta_4),\zeta_4\right), \end{aligned} \tag{37}$$

with the Jacobi-sine function $\mathrm{sn}(u,k)$ from the Appendix B. In an analogous way we find the locations of the voltage taps D,F in the ζ-plane,

$$\begin{aligned} \frac{\zeta_2}{\zeta_4} &= -\mathrm{sn}\left(\left(1-\frac{\varphi_2}{\pi}\right)K(\zeta_4),\zeta_4\right), \\ \frac{\zeta_3}{\zeta_4} &= -\mathrm{sn}\left(\left(1-\frac{\varphi_3}{\pi}\right)K(\zeta_4),\zeta_4\right). \end{aligned} \tag{38}$$

A final transformation maps the upper half of the ζ-plane onto the infinite stripe in the *t*-plane in **Figure 4(d)**,

$$t=c_3\int\frac{(\zeta-\zeta_5)(\zeta+\zeta_5)\mathrm{d}\zeta}{(\zeta-\zeta_0)\sqrt{\zeta-\zeta_4}\sqrt{\zeta-1}\sqrt{\zeta+1}\sqrt{\zeta+\zeta_4}(\zeta+\zeta_0)}+c_4. \tag{39}$$

The point of the input current is at $t_G\to\infty$, the point of the output current is at $t_C\to-\infty$. The structure is folded in such a way that the large contacts $\overline{HJ}$ and $\overline{AB}$ are placed back to back: current $I_{01}(1-\varphi_1/\pi)$ exits the right upper part of the stripe through contact $\overline{HJ}$ and it enters the left upper part of the stripe through contact $\overline{AB}$. The hole degenerates to a slit $\overline{MK}$ with zero width. The slit is aligned in current flow direction. The points K and M are the stagnation points of the current flow pattern. The exterior angles at points t_G,t_C are π, at points t_K,t_M they are $-\pi$, which brings the terms $(\zeta\pm\zeta_5)$ to the numerator and the terms $(\zeta\pm\zeta_0)$ to the denominator of the integrand in (39). The ultimate goal of all these transformations is to achieve homogeneous current density in the stripe in the *t*-plane. Then the distance between points t_D and t_F gives the voltage V_{32}. There are still two unknowns c_3,ζ_5 to be determined. With ζ_5 we make the width of the slit zero,

$$\begin{aligned} t_J-t_L &= 0=c_3\int_\infty^1\frac{(\zeta-\zeta_5)(\zeta+\zeta_5)\mathrm{d}\zeta}{(\zeta-\zeta_0)\sqrt{\zeta-\zeta_4}\sqrt{\zeta-1}\sqrt{\zeta+1}\sqrt{\zeta+\zeta_4}(\zeta+\zeta_0)} \\ &\Rightarrow\int_1^\infty\frac{\mathrm{d}\zeta}{\sqrt{\zeta^2-1}\sqrt{\zeta^2-\zeta_4^2}}+\int_1^\infty\frac{(\zeta_0^2-\zeta_5^2)\mathrm{d}\zeta}{(\zeta^2-\zeta_0^2)\sqrt{\zeta^2-1}\sqrt{\zeta^2-\zeta_4^2}}=0. \end{aligned} \tag{40}$$

With the substitution $x=1/\zeta$ and with [19] this gives

$$\frac{\zeta_5^2-\zeta_0^2}{\zeta_0^2}=\frac{K(\zeta_4)}{\Pi(\zeta_0^2,\zeta_4)-K(\zeta_4)}, \tag{41}$$

with the complete elliptic integral of the third kind $\Pi(\zeta_0^2,\zeta_4)$ (see Appendix B). The scaling constant c_3 follows from

$$i(t_H-t_E)=i=c_3\int_{\zeta_0-}^{\zeta_0+}\frac{(\zeta^2-\zeta_5^2)\mathrm{d}\zeta}{(\zeta^2-\zeta_0^2)\sqrt{\zeta-\zeta_4}\sqrt{\zeta-1}\sqrt{\zeta+1}\sqrt{\zeta+\zeta_4}}, \tag{42}$$

whereby the integration path is an infinitely small semi-circle around ζ_0, *i.e.*, $\zeta=\zeta_0+\varepsilon\exp(i\varphi)$ with $\varepsilon\to 0$ and $\varphi:\pi\to 0$ (see **Figure 4(c)**). We arbitrarily choose the width of the stripe equal to 1. With $\mathrm{d}\zeta=\varepsilon i\exp(i\varphi)\mathrm{d}\varphi$ it follows

$$\begin{aligned}i&=c_3\int_{\pi}^{0}\frac{(\zeta_0^2-\zeta_5^2)\varepsilon i\exp(i\varphi)\mathrm{d}\varphi}{\varepsilon\exp(i\varphi)2\zeta_0\sqrt{\zeta_0-\zeta_4}\sqrt{\zeta_0-1}\sqrt{\zeta_0+1}\sqrt{\zeta_0+\zeta_4}}\\&=c_3\frac{-i\pi(\zeta_0^2-\zeta_5^2)}{2\zeta_0\sqrt{\zeta_4^2-\zeta_0^2}\sqrt{1-\zeta_0^2}},\end{aligned} \tag{43}$$

from which we get c_3. The measured voltage is $V_{32}=I_{01}R_{\text{sheet}}(t_F-t_D)/|t_H-t_E|$ with

$$t_F-t_D=c_3\int_{\zeta_2}^{\zeta_3}\frac{(\zeta^2-\zeta_5^2)\mathrm{d}\zeta}{(\zeta^2-\zeta_0^2)\sqrt{\zeta-\zeta_4}\sqrt{\zeta-1}\sqrt{\zeta+1}\sqrt{\zeta+\zeta_4}}, \tag{44}$$

which is split up in two integrals

$$\int_{\zeta_2}^{\zeta_3}\frac{\mathrm{d}\zeta}{\sqrt{1-\zeta^2}\sqrt{\zeta_4^2-\zeta^2}}=F\left(\frac{\zeta_3}{\zeta_4},\zeta_4\right)-F\left(\frac{\zeta_2}{\zeta_4},\zeta_4\right)=\frac{\varphi_3-\varphi_2}{\pi}K(\zeta_4), \tag{45}$$

(the equality at the right side comes from (113) and (38)) and

$$\begin{aligned}&\int_{\zeta_2}^{\zeta_3}\frac{\mathrm{d}\zeta}{(\zeta_0^2-\zeta^2)\sqrt{1-\zeta^2}\sqrt{\zeta_4^2-\zeta^2}}\\&=\frac{1}{\zeta_0^2}\left(\Pi\left(\arcsin\left(\frac{\zeta_3}{\zeta_4}\right),\frac{\zeta_4^2}{\zeta_0^2},\zeta_4\right)-\Pi\left(\arcsin\left(\frac{\zeta_2}{\zeta_4}\right),\frac{\zeta_4^2}{\zeta_0^2},\zeta_4\right)\right).\end{aligned} \tag{46}$$

Both integrals (45) and (46) are solved by substituting $\zeta=1/x$. $\Pi(w,n,k)$ is the incomplete elliptic integral of the third kind (see Appendix B). Summing up the results of (43) - (46) gives the trans-resistance as a function of parameters in the ζ-plane,

$$\begin{aligned}\frac{R_{01,23}}{R_{\text{sheet}}}&=\frac{V_{32}}{R_{\text{sheet}}I_{01}}=\frac{2}{\pi}\frac{\sqrt{\zeta_4^2-\zeta_0^2}\sqrt{1-\zeta_0^2}}{\zeta_0}\left\{\left(\frac{\Pi(\zeta_0^2,\zeta_4)}{K(\zeta_4)}-1\right)\right.\\&\left.\times\left(F\left(\frac{\zeta_3}{\zeta_4},\zeta_4\right)-F\left(\frac{\zeta_2}{\zeta_4},\zeta_4\right)\right)+\Pi\left(\frac{\zeta_3}{\zeta_4},\frac{\zeta_4^2}{\zeta_0^2},\zeta_4\right)-\Pi\left(\frac{\zeta_2}{\zeta_4},\frac{\zeta_4^2}{\zeta_0^2},\zeta_4\right)\right\}.\end{aligned} \tag{47}$$

The hole size is reflected by ζ_4 (see (36)), and the three azimuthal positions of the point contacts are given by ζ_0,ζ_2,ζ_3 (see (37), (39)). Expressing the trans-resistance in terms of the physical parameters $\varphi_1,\varphi_2,\varphi_3,r_1$ gives

$$
\begin{aligned}
&\frac{R_{01,23}}{R_{\text{sheet}}}=\frac{2}{\pi}\frac{\text{dn}_1}{\text{sc}_1}\left\{\left(\Pi\left(1-\text{dn}_1^2,k\right)-K\right)\frac{\varphi_3-\varphi_2}{\pi}\right.\\
&\qquad\left.+\Pi\left(\text{sn}_2,\frac{1}{\text{sn}_1^2},k\right)-\Pi\left(\text{sn}_3,\frac{1}{\text{sn}_1^2},k\right)\right\},\\
&\text{sn}_1=\text{sn}\left(\left(1-\frac{\varphi_1}{\pi}\right)K,k\right)\quad\text{and}\quad\text{cn}_1=\text{cn}\left(\left(1-\frac{\varphi_1}{\pi}\right)K,k\right)\\
&\text{sc}_1=\text{sn}_1/\text{cn}_1\quad\text{and}\quad\text{dn}_1=\sqrt{1-k^2\text{sn}_1^2}\\
&\text{sn}_2=\text{sn}\left(\left(1-\frac{\varphi_2}{\pi}\right)K,k\right)\quad\text{and}\quad\text{sn}_3=\text{sn}\left(\left(1-\frac{\varphi_3}{\pi}\right)K,k\right)\\
&k=\zeta_4=\sqrt{L\left(\frac{\left|\ln\left(r_1\right)\right|}{\pi}\right)}\quad\text{and}\quad K=K(k).
\end{aligned}
\tag{48}
$$

In (48) sn, cn, dn are Jacobi functions (see Appendix B). The modular lambda elliptic function L simply scales $r_1\mapsto k$ in a highly non-linear way. For the second trans-resistance we can use the replacements (13) in (48). With these formulae for the trans-resistances $R_{01,23}$ and $R_{12,30}$ we will proof two basic properties of doubly-connected plates with peripheral point contacts in the following sections.

3.2. Proof of the Upper Envelope

The *upper* envelope was first conjectured in [9]. It reads

$$\text{vdP}\le 1, \tag{49}$$

for arbitrary placement of the point-contacts on the outer perimeter of a Hall-plate with one insulated hole of arbitrary size. The inequality (49) was proven recently in [14] by arguments using the prime function and Fay's trisecant identity. This Section presents an alternative proof based on the conformal mapping in **Figure 4(d)**. It is short and elegant and it needs no numerical computations.

We start with a general contact arrangement in **Figure 4(a)**,

$$
\begin{aligned}
&0<\varphi_1\le\pi/2\quad\wedge\quad\varphi_1<\varphi_2<\varphi_3<2\pi-\varphi_1,\\
&C=\exp(i\varphi_1),\quad D=\exp(i\varphi_2),\quad F=\exp(i\varphi_3),\quad G=\exp(-i\varphi_1).
\end{aligned}
\tag{50}
$$

If accidentally $\varphi_1>\pi/2$ we shift all contacts by one instance to get $\varphi_1\le\pi/2$. The current splits in two parts, one flowing left around the hole and the other one flowing right around the hole. Thus, there must be a point F' right of the hole, which has the same potential as point F (=contact C_3) left of the hole. There must also be a point D' right of the hole, which has the same potential as point D (=contact C_2) left of the hole. Let us call the potential in point F V_3, in point D V_2, in point F' $V_{3'}$, and in point D' $V_{2'}$. Then it holds $V_{32}=V_{3'2'}$ and this means $R_{01,23}=R_{01,2'3'}$. In **Figure 4(d)** we can easily localize points F' and D'. Point F' has the same horizontal position as point F, however, point F' is on the upper edge of the stripe, whereas point F is on the lower edge. The same applies to points D and D'.

When the second trans-resistance $R_{12,30}$ is measured, current flows between points C (=contact C_1) and D (=contact C_2) and the voltage is measured between points G (=contact C_0) and F (=contact C_3). Analogously, for $R_{12',3'0}$ current flows between points C and D' and the voltage is tapped between points G and F'. However, Figures 4(a)-(d) do not apply in this case, because now the potential distribution is asymmetric. Hence the potential along the straight line $\overline{HJ}$ is *not* constant and therefore we are not allowed to insert an extended contact there. In fact we have to step back to (31) which maps the annulus of Figure 1 *without* a cut and *without* large contacts $\overline{AB}, \overline{HJ}$ to an infinite stripe made up of rectangles like in Figure 4(b) lined up along the $\Im\{w\}$-direction yet without the extended contacts. Instead of the annulus we can think of a helical track that winds around the out-of-plane axis of Figure 1 infinitely often, whereby all four contacts repeat after every full revolution. This is shown in Figure 5(a), where we have infinitely many current and voltage contacts, each ones shorted with a pole, and the potential is periodic in each turn of the spiral. The first turn of the spiral for azimuthal angles $0 \le \varphi < 2\pi$ is called the Riemann sheet #0. It is followed by Riemann sheet #1 for azimuthal angles $2\pi \le \varphi < 4\pi$ and it is preceded by Riemann sheet $\#(-1)$ for azimuthal angles $-2\pi \le \varphi < 0$. This trick extablishes an equivalence between the doubly-connected domain in Figure 1 and the infinite singly-connected domain in Figure 5(a) (in

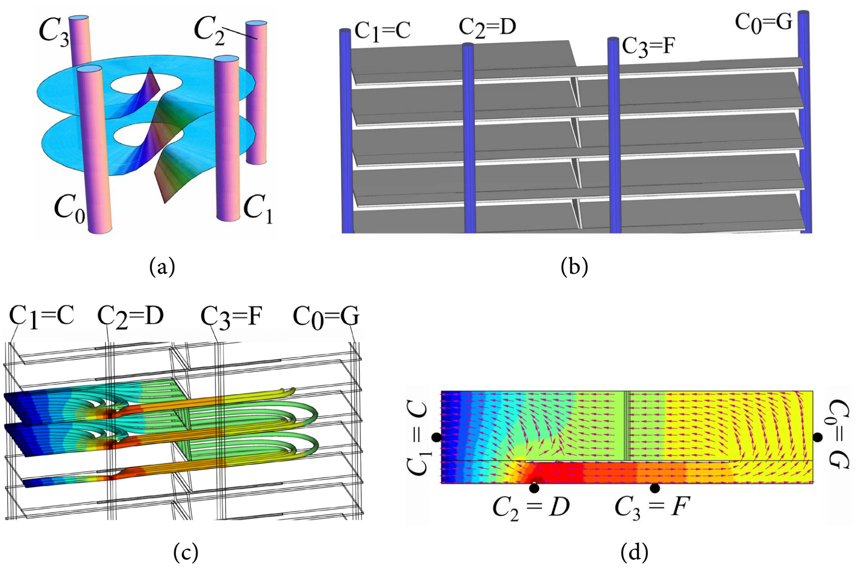

Figure 5. Helical and multi-storey surfaces can represent doubly-connected Hall-plates. The potential in each loop or storey is periodic. The poles short the respective contacts in all loops and storeys. The plots are meant only as an illustration of the infinite number of Riemann sheets. (a) Two loops of an infinite helical Hall-plate. Each loop corresponds to a new Riemann sheet. The poles are contacts C_0, C_1, C_2, C_3; (b) A multi-storey Hall-plate, each storey corresponds to a new Riemann sheet. The four poles are contacts C_0, C_1, C_2, C_3. Note the tiny slits across a major part of the width in all storeys; (c) Current streamlines in two storeys of the multi-storey Hall-plate if current flows from C_2 to C_1; (d) Top view on current vectors and potential in the multi-storey Hall-plate if current flows from C_2 to C_1. Note the current flowing smoothly around the longitudinal slit.

fact we may also consider it doubly-connected because it closes at infinity, thus we have shifted the closure to infinity). Applying the transformation (31) to Figure 1 gives an infinite stripe made up of infinitely many replications of the rectangle of Figure 4(b) with all its contacts. The Schwartz-Christoffel transformation (32) maps this infinite stripe to infinitely many Riemann sheets, which all look like in Figure 4(c), yet the potentials along $\overline{AB}$ and $\overline{HJ}$ are not homogeneous. Instead, Riemann sheet #0 is connected to Riemann sheet #1 along $\overline{HJ}$ and it is connected to Riemann sheet $\#(-1)$ along $\overline{AB}$. The final mapping (39) gives a structure like in Figure 5(b), which comprises infinitely many storeys. Each storey represents one Riemann sheet. Each storey is connected to the upper one along $\overline{HJ}$ and to the lower one through $\overline{AB}$ of Figure 4(d). The voltage and current contacts are at identical positions in all storeys, and the potential is identical in all storeys. This justifies our last step, where we collaps all storeys to a single one, whereby we can join the loose ends $\overline{AB}$ with $\overline{HJ}$ in such a way that A coincides with J and B coincides with H. This final domain is identical to the one in Figure 4(d) with the only difference that the potential along line $\overline{AB} = \overline{HJ}$ is not homogeneous, and therefore the contacts $\overline{AB}, \overline{HJ}$ are deleted and the edges $\overline{AB}, \overline{HJ}$ are glued together. This is shown in Figure 6.

Now we consider the measurement of $R_{12,30}$ in Figure 6. Thereby, current flows between $C_1 = C$ and $C_2 = D$. We may choose the polarity of the current arbitrarily, for physical intuition it might be simpler to inject the current in point D instead of point C and extract it at point C instead of D. Analogously, $R_{12',3'0}$ is measured by injecting current at point D', extracting it at point C, and measuring the voltage between points F' and G. Now the slit plays a decisive role: since we started with $0 < \varphi_1 \le \pi/2$ the slit in Figure 6 is closer to the lower edge with points D, F than to the upper edge with points D', F'. The slit represents an obstacle to the current flow, and therefore the voltage between points F, G must be larger than the voltage between points F', G. Hence, it holds $R_{12,30} > R_{12',3'0}$.

The reciprocity principle [20] says that at zero magnetic field the voltage between $F'D'$ for current flowing between GC is identical to the voltage between

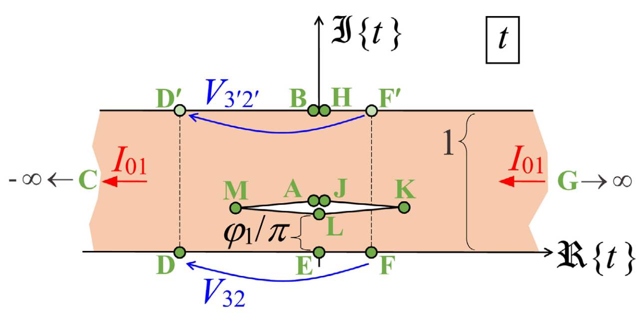

Figure 6. Annular Hall-plate in the t-plane with longitudinal slit. Current may flow between arbitrary contacts $C_0 = G, C_1 = C, C_2 = D, C_3 = F$, in this example the current flows from G to C, which gives a homogeneous current density with $V_{32} = V_{3'2'}$.

GC for current flowing between $F'D'$. In fact this also holds in the presence of a magnetic field as long as the entire boundary is insulating with all point-sized current contacts on the same boundary with G and C being neighbours as well as F' and D', see Section 4.

To sum up, we have two sets of contacts in **Figure 1**, the original points C_0, C_1, C_2, C_3 and the new points $C_{3'}, C_{2'}, C_1, C_0$, whereby the first trans-resistances are identical, $R_{01,23} = R_{3'2',10}$, but the second trans-resistance is smaller for the new points, $R_{2'1,03'} < R_{12,30}$.

I call this transformation $C_0, C_1, C_2, C_3 \rightarrow C_{3'}, C_{2'}, C_1, C_0$ a *contraction*, because the new points are closer together than the old ones.

Let us repeat the contraction process infinitely often, until all four contacts are infinitely close together.

In this limit the contacts are so close together that the current arcs between the current contacts are tiny. Then the hole is comparatively distant and it does not affect the current distribution any more. Thus the potentials at the voltage contacts become identical to the potentials in a singly-connected Hall plate.

However, for singly-connected Hall plates the van der Pauw Equation (3) holds. Since the second trans-resistance decreased during the contraction process, the inequality (49) must hold before contraction. This completes the proof.

The essential step in the proof was to show that $R_{12',3'0} < R_{12,30}$ holds. To this end we used the arguments of the multi-storey Hall-plate in **Figure 5** to justify **Figure 6**, in which the slit was a bigger obstacle for $R_{12,30}$ than for $R_{12',3'0}$. We can avoid the use of multi-storey Hall-plates by the following line of arguments. We use **Figure 1**. In the measurement of $R_{12,30}$ current I_{12} flows from C_1 to C_2 and voltage V_{03} is tapped. Thereby a first current $I_{12}(\varphi_2 - \varphi_1)/(2\pi)$ flows *clockwise* around the hole [17]. In the measurement of $R_{12',3'0}$ we inject the same current I_{12} into C_1 and extract it at $C_{2'}$ and we tap the voltage $V_{03'}$. Thereby a second current $I_{12}(\varphi_1 - \varphi_{2'})/(2\pi)$ flows *counter-clockwise* around the hole, whereby $\varphi_{2'}$ is the azimuthal position of $C_{2'}$. If $C_{2'}$ is in the lower half of the *z*-plane it holds $\varphi_1 - \varphi_{2'} < 0$ and then the current is $I_{12}(\varphi_1 + 2\pi - \varphi_{2'})/(2\pi)$. We have to prove that $V_{03'} < V_{03}$. Per definition, the point $C_{2'}$ was obtained from C_2 by a contraction process, therefore it holds $\varphi_1 - \varphi_{2'} < \varphi_2 - \varphi_1$. If $C_{2'}$ is in the lower half of the *z*-plane it holds $\varphi_1 + 2\pi - \varphi_{2'} < \varphi_2 - \varphi_1$. Consequently, in any case the first current is larger than the second current, because C_2 is more distant from C_1 than $C_{2'}$ is from C_1. If we superimpose both measurements, identical currents I_{12} flow simultaneously from C_1 to C_2 and from C_1 to $C_{2'}$ and a positive net current flows *clockwise* around the hole in a direction from $C_{3'}$ towards C_3. Since there are no current sources except in $C_1, C_2, C_{2'}$ the potential drops monotonically along the clockwise current streamline on the outer perimeter from $C_{3'}$ to C_3. This means $V_{3'} > V_3$, which means $V_{03'} < V_{03}$, which again completes this proof.

3.3. Derivation of the Lower Envelope

The upper envelope theorem implies that for any doubly-connected Hall-plate we can find a $\star$-configuration which has the same trans-resistances $R_{01,23}, R_{12,30}$ and the same sheet resistance. This is not a specific property of $\star$-configurations. Also other contact patterns have the same property: e.g. contacts with $\varphi_1 = \pi/2 < \varphi_2 < \pi$ and $\pi - \varphi_2 = \varphi_3 - \pi$, let us call them *type 2 configurations*, are also able to assume any physically meaningful pairs of values for the two trans-resistances (see Figure 7).

In the van der Pauw plane of Figure 7, a specific Hall-plate is represented by a dot. During the contraction process (c.p.) this point moves vertically up in the van der Pauw plane until it finally is on the straight line $Y = 1 - X$, which is the upper envelope (u.e.). If we reverse the contraction process we can expand the contact arrangement, whereby the point moves down in the van der Pauw plane. However, this *expansion process* (e.p.) stops when the spacing between the current contacts, $C_0 - C_1$, is larger than the spacings of all other neighbouring contacts, $C_1 - C_2, C_2 - C_3, C_3 - C_0$, and the voltage contacts are in the obtuse angle of the current contacts. This brings us in a natural way to the question of the smallest possible Y and the smallest possible $\text{vdP} = X + Y$ for fixed X. For the $\star$-configuration of contacts we know that the van der Pauw function decreases with larger holes and for $\varphi_1 \to \pi/4$. On the other hand, the van der Pauw function tends to its maximum of 1 if only the contact arrangement is contracted sufficiently, or if $\varphi_1 \to 0 \vee \varphi_1 \to \pi/2$ in a $\star$-configuration. Then, one trans-resistance goes to infinity and the other one to zero. Thus, the question arises, what is the minimum van der Pauw function, if the hole *and* one trans-resistance are fixed. In other words, what are the maximum second trans-resistance and its associated contact locations? For every arbitrarily chosen first trans-resistance we get a maximum second trans-resistance. The set of all these pairs is called the *lower envelope* (l.e), because all Hall-plates with a fixed Riemann modulus are repesented by points between upper and lower envelopes.

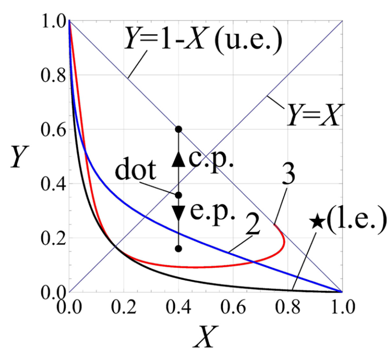

Figure 7. In the van der Pauw plane (X, Y) each Hall-plate is represented by a dot. It moves up in the contraction process (c.p.) and down in the expansion process (e.p.). The upper envelope (u.e.) is the line $Y = 1 - X$. The lower envelope (l.e) is given by (69). Type 2 and type 3 contact arrangements give the curves 2 and 3, respectively. The three curves $(\star, 2, 3)$ assume a hole of size $r_1 = 1/2$.

[9] conjectured that the lower envelope is given by $\star$-contact arrangements and this was also proven in [14]. For small holes, our derivation of (21) leads straight to the same conjecture. A precise statement of the lower envelope reads:

For a fixed trans-resistance $R_{01,23}$ the arrangement of the point contacts for largest $R_{12,30}$ is a $\star$-arrangement.

3.4. A Proof of the Lower Envelope

In mathematical terms the lower envelope is defined like this:

Equation (48) gives $R_{01,23}$ as a function of the contacts' positions $\varphi_1, \varphi_2, \varphi_3$. If $R_{01,23}$ has to remain constant, this defines $\varphi_1(\varphi_2, \varphi_3)$ as an implicit function of φ_2 and φ_3. If we compute $R_{12,30}$ analogous to (48) and insert the implicit function of $\varphi_1(\varphi_2, \varphi_3)$, this gives a function of two degrees of freedom, $R_{12,30}(\varphi_2, \varphi_3)$. We want to prove that this function assumes a unique maximum if $\varphi_2 = \pi - \varphi_1$ and $\varphi_3 = \pi + \varphi_1$, which is the $\star$-configuration as it is defined in (21).

Put in another way,

$$\begin{aligned}
&\frac{\partial R_{01,23}\left(\varphi_1\left(\varphi_2,\varphi_3\right),\varphi_2,\varphi_3\right)}{\partial \varphi_2} = 0, \quad \frac{\partial R_{01,23}\left(\varphi_1\left(\varphi_2,\varphi_3\right),\varphi_2,\varphi_3\right)}{\partial \varphi_3} = 0, \\
&\frac{\partial R_{12,30}\left(\varphi_1\left(\varphi_2,\varphi_3\right),\varphi_2,\varphi_3\right)}{\partial \varphi_2} = 0, \quad \frac{\partial R_{12,30}\left(\varphi_1\left(\varphi_2,\varphi_3\right),\varphi_2,\varphi_3\right)}{\partial \varphi_3} = 0, \\
&\text{for } \varphi_2 = \pi - \varphi_1 \quad \text{and} \quad \varphi_3 = \pi + \varphi_1 \quad \text{and} \quad 0 < \varphi_1 \le \pi/2,
\end{aligned} \tag{51}$$

whereby the first line of (51) reflects the constancy of trans-resistance $R_{01,23}$ and the second line defines the extremum of $R_{12,30}$. The proof gets simpler if we apply the following transformations. Instead of the free parameters $\varphi_1, \varphi_2, \varphi_3$ we use (37), (38) and (113) to introduce new parameters F_0, F_2, F_3,

$$\begin{aligned}
F_0 &= F\left(\frac{\zeta_0}{k}, k\right) = \left(1 - \frac{\varphi_1}{\pi}\right) K, \\
F_2 &= F\left(\frac{\zeta_2}{k}, k\right) = -\left(1 - \frac{\varphi_2}{\pi}\right) K, \\
F_3 &= F\left(\frac{\zeta_3}{k}, k\right) = -\left(1 - \frac{\varphi_3}{\pi}\right) K,
\end{aligned} \tag{52}$$

with $K = K(k)$ and $k = \zeta_4$ like in (48). From (50) it follows

$$\pi/4 \le K/2 \le F_0 < K \quad \text{and} \quad -F_0 < F_2 < F_3 < F_0. \tag{53}$$

The replacements (13) were used to compute $R_{12,30}$ with the same formula as $R_{01,23}$. In terms of the new parameters F_0, F_2, F_3 the replacement rules become

$$\begin{aligned}
F_0 &\mapsto K - F_0/2 - F_2/2 \\
F_2 &\mapsto -K + F_0/2 - F_2/2 + F_3 \\
F_3 &\mapsto -K + 3F_0/2 - F_2/2.
\end{aligned} \tag{54}$$

Analogous to (21) the $\star$-configuration is specified by

$$\pi/4 \le K/2 \le F_0^\star < K \quad \text{and} \quad F_2^\star = -F_3^\star = F_0^\star - K. \tag{55}$$

We define the following function

$$f(x,y,z)=\frac{\mathrm{dn}(x)}{\mathrm{sc}(x)}\left\{\left(\Pi\left(1-\mathrm{dn}^2(x),k\right)-K\right)\frac{z-y}{K}\right.$$
$$\left.+\Pi\left(\mathrm{sn}(z),\frac{1}{\mathrm{sn}^2(x)},k\right)-\Pi\left(\mathrm{sn}(y),\frac{1}{\mathrm{sn}^2(x)},k\right)\right\},\quad (56)$$

where we skipped the second argument in the Jacobi functions, e.g., $\mathrm{sn}(x)=\mathrm{sn}(x,k)$. With (48) it holds

$$\frac{R_{01,23}}{R_{\text{sheet}}}=\frac{2}{\pi}f(F_0,F_2,F_3)$$
$$\frac{R_{12,30}}{R_{\text{sheet}}}=\frac{2}{\pi}f\left(K-\frac{F_0+F_2}{2},\frac{F_0-F_2}{2}+F_3-K,\frac{3F_0-F_2}{2}-K\right).\quad (57)$$

The first part of the upper envelope theorem requires constant $R_{01,23}$, which means $\mathrm{d}f(F_0,F_2,F_3)=0$ with the implicit function $F_0=F_0(F_2,F_3)$. This gives

$$f^{(1,0,0)}(F_0,F_2,F_3)\frac{\partial F_0}{\partial F_2}+f^{(0,1,0)}(F_0,F_2,F_3)=0$$
$$f^{(1,0,0)}(F_0,F_2,F_3)\frac{\partial F_0}{\partial F_3}+f^{(0,0,1)}(F_0,F_2,F_3)=0,\quad (58)$$

in $\star$-configuration, which is in $F_0=F_0^\star$, $F_2=F_0^\star-K$, $F_3=-F_0^\star+K$ according to (55). From (56) it follows

$$f^{(0,1,0)}(x,y,z)=-f^{(0,0,1)}(x,y,z).\quad (59)$$

Inserting this into (58) and adding up both equations gives

$$\frac{\partial F_0}{\partial F_2}=-\frac{\partial F_0}{\partial F_3}.\quad (60)$$

Inserting (59) into the second line of (58) gives

$$\frac{\partial F_0}{\partial F_3}=\frac{f^{(0,1,0)}\left(F_0^\star,F_0^\star-K,K-F_0^\star\right)}{f^{(1,0,0)}\left(F_0^\star,F_0^\star-K,K-F_0^\star\right)}.\quad (61)$$

The second part of the upper envelope theorem says that $R_{12,30}$ has an extremum, which means $\mathrm{d}f\left(K-F_0/2-F_2/2,F_0/2-F_2/2+F_3-K,3F_0/2-F_2/2-K\right)=0$ in $\star$-configuration with $F_0=F_0^\star,F_2=F_0^\star-K,F_3=K-F_0^\star$ according to (55). This gives

$$\left(\frac{-1}{2}\frac{\partial F_0}{\partial F_2}-\frac{1}{2}\right)f^{(1,0,0)}+\left(\frac{1}{2}\frac{\partial F_0}{\partial F_2}-\frac{1}{2}\right)f^{(0,1,0)}+\left(\frac{3}{2}\frac{\partial F_0}{\partial F_2}-\frac{1}{2}\right)f^{(0,0,1)}=0,$$
$$\frac{-1}{2}\frac{\partial F_0}{\partial F_3}f^{(1,0,0)}+\left(\frac{1}{2}\frac{\partial F_0}{\partial F_3}+1\right)f^{(0,1,0)}+\frac{3}{2}\frac{\partial F_0}{\partial F_3}f^{(0,0,1)}=0\quad (62)$$

in $\star$-configuration. Adding both equations and using (59) and (60) gives

$$\frac{1}{2}=\frac{f^{(0,1,0)}\left(3K/2-F_0^\star,K/2-F_0^\star,F_0^\star-K/2\right)}{f^{(1,0,0)}\left(3K/2-F_0^\star,K/2-F_0^\star,F_0^\star-K/2\right)}.\quad (63)$$

Re-inserting this into the first equation of (62) gives

$$\frac{\partial F_0}{\partial F_3} = \frac{1}{2}. \tag{64}$$

Combining (64) and (61) gives

$$\frac{1}{2} = \frac{f^{(0,1,0)}\left(F_0^\star, F_0^\star - K, K - F_0^\star\right)}{f^{(1,0,0)}\left(F_0^\star, F_0^\star - K, K - F_0^\star\right)}. \tag{65}$$

To sum up, we have to proof the validity of (63) and (65). From the contraction process we know that the extremum of $R_{12,30}$ cannot be a minimum, it must be a maximum. The nice feature is that both equations have an identical shape, they differ only in the test point x_0. Thus we only have to prove

$$\frac{1}{2} = \frac{f^{(0,1,0)}\left(x_0, x_0 - K, K - x_0\right)}{f^{(1,0,0)}\left(x_0, x_0 - K, K - x_0\right)} \quad \text{for } \frac{K}{2} \le x_0 < K. \tag{66}$$

From the reciprocity principle in [20] we know that $R_{01,23}$ remains constant if we swap current and voltage contacts. This gives

$$f\left(x, y, z\right) = f\left(K - \frac{z-y}{2}, x - K - \frac{y+z}{2}, K - x - \frac{y+z}{2}\right). \tag{67}$$

Combining (67) and (59) gives

$$f^{(1,0,0)}\left(x, y, z\right) = 2 f^{(0,1,0)}\left(K - \frac{z-y}{2}, x - K - \frac{y+z}{2}, K - x - \frac{y+z}{2}\right). \tag{68}$$

For a Hall-plate with contacts in $\star$-configuration it holds $x \to x_0, y \to x_0 - K, z \to K - x_0$, see (55). Inserting this into (68) gives (66), which completes the proof. An alternative proof of (66) is given in Appendix C.

3.5. The Minimum of the Van Der Pauw Function

With (57) and (55) the lower envelope curve in the van der Pauw plane is parametrized in a closed formula as follows,

$$\begin{aligned} &X \to X^\star = \exp\left(-2f\left(F_0^\star, F_0^\star - K, K - F_0^\star\right)\right), \\ &Y \to Y^\star = \exp\left(-2f\left(3K/2 - F_0^\star, K/2 - F_0^\star, F_0^\star - K/2\right)\right), \\ &\text{for } K/2 \le F_0^\star < K \ \text{ and } \ K = K\left(\zeta_4\right). \end{aligned} \tag{69}$$

The lower envelope is identical to general $\star$-configurations with $0 < \varphi_1 \le \pi/2$ (insert the first line of (52) into (69)). For the specific $\star$-configuration with $\varphi_1 = \pi/4, \varphi_2 = 3\pi/4, \varphi_3 = 5\pi/4$ the van der Pauw function has its minimum,

$$\text{vdP}\left(\varphi_1, \varphi_2, \varphi_3, r_1\right) \ge \text{vdP}_{\min}\left(r_1\right) = 2\exp\left(-2f\left(3K/4, -K/4, K/4\right)\right), \tag{70}$$

whereby $K = K\left(k\right)$ depends only on the Riemann modulus r_1 (see (48)). Figure 8 shows this function. It is close to 1 for $r_1 < 0.1$ and it is very close to 0 for $r_1 > 0.8$.

The lower envelope theorem marks the outstanding position of the $\star$-Hall-plates: if the two values $R_{01,23}/R_{\text{sheet}}$, $R_{12,30}/R_{\text{sheet}}$ are given, we can find a $\star$-arrangement that fits to them, and we can be sure that there is no other

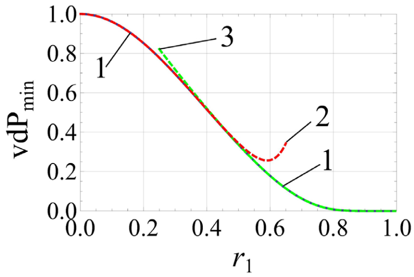

Figure 8. The plot shows the minimum of the van der Pauw function $\mathrm{vdP}_{\min}$ versus hole radius r_1. All possible arrangements of the four point contacts were varied until the minimum was obtained for a specific $\star$-configuration of contacts which is specified by $\varphi_1=\pi/4, \varphi_2=3\pi/4, \varphi_3=5\pi/4$, then the contacts are in the vertices of a square inscribed into the unit circle. The blue curve 1 is the exact Formula (70), the red dashed curve 2 is the small hole approximation (24), and the green dashed curve 3 is the large hole approximation (83). Curve 1 is behind curves 2, 3. Both approximations are very accurate. They have identical values at $r_1=0.4508043$.

contact arrangement with a smaller hole which could give the same values $R_{01,23}/R_{\text{sheet}}$, $R_{12,30}/R_{\text{sheet}}$. Thus, the star-arrangement determines the minimum required hole size to give the measured deviation of the van der Pauw function from 1. Other contact arrangements like the type 2 configuration are also able to produce the same trans-resistances, but they may need larger holes to do so. Conversely, contact arrangements with $\varphi_2=3\varphi_1, \varphi_3=5\varphi_1$, which I call *type 3 configuration*, cannot give very large $R_{12,30}$ and very small $R_{01,23}$ at fixed hole radius r_1, as it is shown in the red curve (3) in **Figure 7**. The type 3 curves go through the point $(X,Y)=(3/4,1/4)$ for $\varphi_1\to 0$ for all hole sizes r_1. Type 3 configuration and $\star$-configuration are similar near $\varphi_1=\pi/4$.

3.6. Some Properties of $f(x,y,z)$ and vdP

The function $f(x,y,z)$ may be expressed in various formulae. We can eliminate the complete elliptic-Pi function in (56) with the help of [21]. We can also pull out a logarithm from the incomplete elliptic-Pi integrals with [22],

$$\begin{aligned}&\Pi\left(\mathrm{sn}(z),\frac{1}{\mathrm{sn}^2(x)},k\right)\\&=\frac{1}{2}\frac{\mathrm{sc}(x)}{\mathrm{dn}(x)}\ln\left(\frac{\mathrm{sn}(x+z)}{\mathrm{sn}(x-z)}\right)+z-\Pi\left(\mathrm{sn}(z),k^2\mathrm{sn}^2(x),k\right).\end{aligned} \tag{71}$$

Here we use again the short-hand writing $\mathrm{sn}(u,k)=\mathrm{sn}(u)$. This gives

$$\begin{aligned}f(x,y,z)=&\frac{1}{2}\ln\left(\frac{\mathrm{sn}(x+z)}{\mathrm{sn}(x-z)}\frac{\mathrm{sn}(x-y)}{\mathrm{sn}(x+y)}\right)+(z-y)Z(\mathrm{sn}(x),k)\\&+\frac{\mathrm{dn}(x)}{\mathrm{sc}(x)}\left(z-y-\Pi\left(\mathrm{sn}(z),k^2\mathrm{sn}^2(x),k\right)+\Pi\left(\mathrm{sn}(y),k^2\mathrm{sn}^2(x),k\right)\right).\end{aligned} \tag{72}$$

$Z(u,k)$ is the Jacobi-zeta function defined in (111). For vanishing hole,

$r_1 = 0 \Rightarrow k = 0$, only the logarithmic term in (72) remains. With [23],

$$\begin{aligned} &yE(\mathrm{sn}(x),k) - xE(\mathrm{sn}(y),k) \\ &= \frac{\mathrm{dn}(x)}{\mathrm{sc}(x)}\left(\Pi\left(\mathrm{sn}(y),k^2\mathrm{sn}^2(x),k\right)-y\right) - \frac{\mathrm{dn}(y)}{\mathrm{sc}(y)}\left(\Pi\left(\mathrm{sn}(x),k^2\mathrm{sn}^2(y),k\right)-x\right), \end{aligned} \tag{73}$$

and with the addition theorems of the Jacobi-zeta function [24] and of the Jacobi-sn function [30] it follows

$$\begin{aligned} &f(x,y,z) \\ &= \frac{1}{2}\ln\left(\frac{\mathrm{sn}(x+z)}{\mathrm{sn}(x-z)}\frac{\mathrm{sn}(x-y)}{\mathrm{sn}(x+y)}\right) + x\left(Z(\mathrm{sn}(z-y),k) - \frac{\mathrm{sn}(z-y)}{\mathrm{sn}(y)\,\mathrm{sn}(z)}\right) \\ &+ \frac{\mathrm{dn}(y)}{\mathrm{sc}(y)}\Pi\left(\mathrm{sn}(x),k^2\mathrm{sn}^2(y),k\right) - \frac{\mathrm{dn}(z)}{\mathrm{sc}(z)}\Pi\left(\mathrm{sn}(x),k^2\mathrm{sn}^2(z),k\right). \end{aligned} \tag{74}$$

Figure 9 shows how the trans-resistances and the van der Pauw function change when the size of the hole grows from zero to full size while the contacts positions remain constant. In the van der Pauw plane of **Figure 9(a)** curves 1, 3 and 4 show that one of the two coordinates X, Y may increase initially before it decreases (the directions of growing r_1 are indicated by the arrows on the curves). Along the other curves, both coordinates X, Y decrease monotonically for all hole sizes $r_1: 0 \to 1$. In the limit of infinitely thin annular regions, all curves end in the origin $(X,Y) = (0,0)$. In all cases, the van der Pauw function vdP decreases monotonically versus r_1, $\partial X/\partial r_1 + \partial Y/\partial r_1 \le 0$, see **Figure 9(b)**. I have no rigorous proof of this conjecture. The plots in **Figure 9(b)** also show that the van der Pauw function may change only little for $r_1 < 0.95$ in curve 3

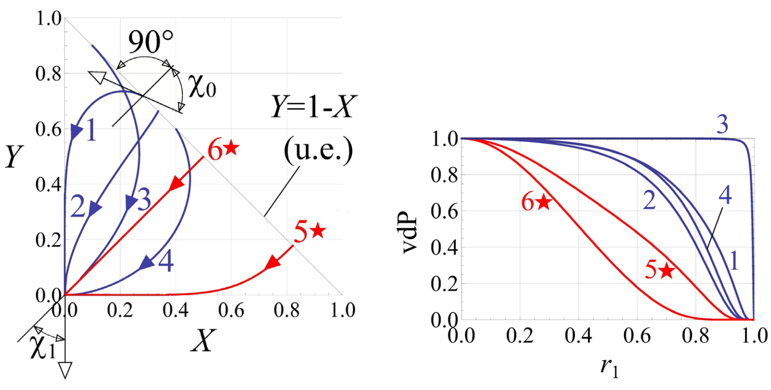

Figure 9. Six Hall-plates with different contacts positions for centered circular holes with increasing size $r_1: 0 \to 1$. Curves 1, 2, 4 have identical $\varphi_1 = 10^\circ$, $\varphi_2 = 20^\circ$, yet φ_3 is 270° for curve 1, 180° for curve 2, and 90° for curve 4. Curve 3 has $\varphi_1 = 0.3\,\mathrm{rad} = 17.189^\circ$, $\varphi_2 = 17.349^\circ$, $\varphi_3 = 18.859^\circ$. Curves $5\star$, $6\star$ are star-configurations with $\varphi_1^* = 25^\circ$ for curve $5\star$ and $\varphi_1^* = 45^\circ$ for curve $6\star$. Curve $6\star$ is identical to $\mathrm{vdP}_{\min}$ from (70). (a) Representation of the six Hall-plates in the van der Pauw plane (X,Y) for $r_1: 0 \to 1$. χ_0, χ_1 are indicated for curve 1; (b) vdP-function of the six Hall-plates versus r_1.

or for $r_1 < 0.4$ (see curves 1, 2, 4) or for $r_1 > 0.8$ (see curve 6). In these cases, the van der Pauw function is not a very sensitive measure to detect holes.

A distinct feature of the curves in **Figure 9(a)** is the angle χ_0 under which they start from the line $Y = 1 - X$. Let us call it the *small-hole-angle*. This angle is between the tangent on the parametric curve $\left(X(r_1), Y(r_1)\right)$ in $r_1 = 0$ and the vector $(-1,-1)^{\mathrm{T}}$. It holds $\chi_0 \in (-\pi/2, \pi/2)$ with

$$\begin{aligned}\cos(\chi_0) &= \frac{1}{\sqrt{\mathrm{d}X_0^2 + \mathrm{d}Y_0^2}} \begin{pmatrix} \mathrm{d}X_0 \\ \mathrm{d}Y_0 \end{pmatrix} \cdot \frac{1}{\sqrt{2}} \begin{pmatrix} -1 \\ -1 \end{pmatrix} \\ &= \frac{1}{\sqrt{2}} \frac{\cos\left(\varphi_1 - (\varphi_3 - \varphi_2)/2\right) - \cos\left((\varphi_2 + \varphi_3)/2\right)}{\sqrt{\cos^2\left(\varphi_1 - (\varphi_3 - \varphi_2)/2\right) + \cos^2\left((\varphi_2 + \varphi_3)/2\right)}},\end{aligned} \tag{75}$$

with $\mathrm{d}X_0, \mathrm{d}Y_0$ from (16). The small-hole-angle χ_0 vanishes for

$$\cos(\chi_0) = 1 \quad \Leftrightarrow \quad \cos\left(\varphi_3 - \varphi_1 - \frac{\varphi_2 + \varphi_3}{2}\right) = -\cos\left(\frac{\varphi_2 + \varphi_3}{2}\right), \tag{76}$$

which has two meaningful solutions

$$\begin{aligned}&\text{case 1}: 0 < \varphi_1 < \varphi_2 = \pi - \varphi_1 < \varphi_3 < 2\pi - \varphi_1, \\ &\text{case 2}: 0 < \varphi_1 < \varphi_2 < \varphi_3 = \pi + \varphi_1 < 2\pi - \varphi_1.\end{aligned} \tag{77}$$

In words, if two non-neighbouring peripheral contacts lie on a straight line through the center of the annular Hall-plate, the curves in **Figure 9(a)** start *perpendicularly* from the upper envelope. This comprises all star-configurations, but it is more general than star-configurations. From (22) we know that for $\star$-configurations in the asymptotic limit of a small hole the van der Pauw function vdP has the steepest decline versus hole size, as a quantity to detect small holes, vdP becomes most sensitive if the contacts are in a $\star$-configuration. Therefore, for small r_1 the red curves $5\star$, $6\star$ are *below* the blue curves 1, 2, 3, 4 in **Figure 9(b)**. If (77) is fullfilled the curves $\left(X(r_1), Y(r_1)\right)$ start perpendicularly from the upper envelope. Yet, there exist contact configurations, which are not $\star$-configurations, but which still fullfill (77). Their curves $\left(X(r_1), Y(r_1)\right)$ also start perpendicularly from the upper envelope, but for them the slope of the van der Pauw function differs from (22),

$$\begin{aligned}&\text{case 1}: \mathrm{vdP} = 1 + 4\sin(2\varphi_1)\sin(\varphi_1 + \varphi_3) r_1^2 + \mathcal{O}(r_1)^4, \\ &\text{case 2}: \mathrm{vdP} = 1 - 4\sin(2\varphi_1)\sin(\varphi_2 - \varphi_1) r_1^2 + \mathcal{O}(r_1)^4.\end{aligned} \tag{78}$$

For $\chi_0 = \pm\pi/2$ the curves $\left(X(r_1), Y(r_1)\right)$ start *tangentially* from the upper envelope. Then it holds

$$\cos(\chi_0) = 0 \quad \Leftrightarrow \quad \cos\left(\varphi_3 - \varphi_1 - \frac{\varphi_2 + \varphi_3}{2}\right) = \cos\left(\frac{\varphi_2 + \varphi_3}{2}\right). \tag{79}$$

This condition is fullfilled only if three or all four contacts approach infinitely closely. From **Figure 9(a)** I surmize that *both trans-resistances are monotonic versus* r_1 as long as $\chi_0 \in [-\pi/4, \pi/4]$. Then it holds

$$\cos(\chi_0) \geq \frac{1}{\sqrt{2}} \quad \Leftrightarrow \quad \cos(\varphi_1 + \varphi_2) + \cos(\varphi_3 - \varphi_1) \leq 0. \tag{80}$$

Inequality (80) is fullfilled for

$$0<\varphi_1\le \pi/2 \wedge \max\left(\varphi_2,\pi-\varphi_2\right)<\varphi_3<\min\left(2\pi-\varphi_1,\pi+2\varphi_1+\varphi_2,3\pi-\varphi_2\right). \quad (81)$$

For the blue curves 1, 2, 3, 4 in **Figure 9(a)** we get $\chi_0=-72.29^\circ$, 18.08˚, 89.74˚, 77.33˚, respectively, whereby I define the sign of χ_0 equal to the sign of $\mathrm{d}X_0-\mathrm{d}Y_0$, this is identical to the sign of $\left(\sin(\varphi_2)-\sin(\varphi_1)\right)\left(\sin(\varphi_1)+\sin(\varphi_3)\right)$.

3.7. The Asymptotic Limit of a Very Large Hole

In the limit $r_1\to 1$ the annular region of the Hall-plate degenerates to an infinitely thin ring. Then the trans-resistances grow unboundedly. We use $k\to 1$ in (57) with (72) to compute the limit of $f(x,y,z)$. With (117) and (118) it follows

$$\begin{aligned}\frac{R_{01,23}}{R_{\text{sheet}}}&=\frac{2\varphi_1(\varphi_3-\varphi_2)}{\pi^3}K\to\frac{\varphi_1(\varphi_2-\varphi_3)}{\pi\ln(r_1)},\\ \frac{R_{12,30}}{R_{\text{sheet}}}&\to\frac{(\varphi_2-\varphi_1)(\varphi_1+\varphi_3-2\pi)}{2\pi\ln(r_1)}.\end{aligned} \quad (82)$$

Inserting (82) into (2) gives

$$\lim_{r_1\to 1}\mathrm{vdP}_{\min}=2\exp\left(\frac{\pi^2}{8\ln(r_1)}\right), \quad (83)$$

which is plotted as the green curve 3 in **Figure 8**. Let us define

$$X_1=\lim_{r_1\to 1}X \quad\text{and}\quad Y_1=\lim_{r_1\to 1}Y. \quad (84)$$

Inserting (82) into (84) with the definitions in (2) leads to

$$Y_1=X_1^{\vartheta}\quad\text{with}\quad \vartheta:=\frac{(\varphi_2-\varphi_1)(2\pi-\varphi_1-\varphi_3)}{2\varphi_1(\varphi_3-\varphi_2)}>0 \quad (85)$$

in the asymptotic case $r_1\to 1$. This tells us at which angle the curves in the van der Pauw plane of **Figure 9(a)** approach the origin. It holds

$$\lim_{X_1\to 0}\frac{\mathrm{d}Y_1}{\mathrm{d}X_1}=\vartheta X_1^{\vartheta-1}=\begin{cases}\infty & \text{for } 0<\vartheta<1\\ 1 & \text{for } \vartheta=1\\ 0 & \text{for } \vartheta>1\end{cases} \quad (86)$$

Let us define the angle χ_1 between the tangent on the parametric curve $\left(X(r_1),Y(r_1)\right)$ in $r_1\to 1$ and the vector $(-1,-1)^{\mathrm{T}}$. I will call it the *large-hole-angle*. It holds $\chi_1\in\{-\pi/4,0,\pi/4\}$ with

$$\begin{aligned}\cos(\chi_1)&=\lim_{X_1\to 0}\frac{1}{\sqrt{1+(\mathrm{d}Y_1/\mathrm{d}X_1)^2}}\begin{pmatrix}-1\\ -\mathrm{d}Y_1/\mathrm{d}X_1\end{pmatrix}\cdot\frac{1}{\sqrt{2}}\begin{pmatrix}-1\\ -1\end{pmatrix}\\ &=\lim_{X_1\to 0}\frac{1}{\sqrt{2}}\frac{1+\vartheta X_1^{\vartheta-1}}{\sqrt{1+\vartheta^2X_1^{2\vartheta-2}}}.\end{aligned} \quad (87)$$

This gives

$$\chi_1=\begin{cases}\pi/4 & \text{for } 0<\vartheta<1\\ 0 & \text{for } \vartheta=1\\ -\pi/4 & \text{for } \vartheta>1\end{cases} \quad (88)$$

whereby I define the sign of χ_1 equal to the sign of $(-1)(1-\mathrm{d}Y_1/\mathrm{d}X_1)$, this is identical to the sign of $1-\vartheta$. For the curves 1 - 6 in **Figure 9(a)** we get $\chi_1 = 45^\circ, 45^\circ, 0^\circ, -45^\circ, -45^\circ, 0^\circ$, respectively. In general, star-arrangements have $\chi_1 = 45^\circ$ for $X < 0.5$, $\chi_1 = 0^\circ$ for $X = 0.5$, and $\chi_1 = -45^\circ$ for $X > 0.5$. (For a star-configuration $X < 0.5$ means $\vartheta < 1$ and $\varphi_1^\star > \pi/4$.) The interesting case $\chi_1 = 0$ corresponds to

$$\varphi_3 = \varphi_1 + 2\pi \frac{\varphi_2 - \varphi_1}{\varphi_2 + \varphi_1}. \tag{89}$$

This holds for a wide class of contact arrangements, including the specific star-configuration with $\varphi_1^\star = \pi/4$. Inserting (89) into the first line of (16) and into (75) gives

$$X_0 = \frac{-\sin\left(\frac{\varphi_2-\varphi_1}{2}\right)\sin\left(\varphi_1 + \pi\frac{\varphi_2-\varphi_1}{\varphi_2+\varphi_1}\right)}{\sin\left(\frac{\varphi_2+\varphi_1}{2}\right)\sin\left(\frac{2\pi\varphi_2}{\varphi_2+\varphi_1}\right)}$$
$$\cos(\chi_0) = \frac{-\sqrt{2}\sin\left(\frac{\varphi_2+\varphi_1}{2}\right)\sin\left(\frac{2\pi\varphi_2}{\varphi_2+\varphi_1}\right)}{\sqrt{1+\cos(\varphi_1+\varphi_2)\cos\left(2\pi\frac{\varphi_2-\varphi_1}{\varphi_2+\varphi_1}\right)}}. \tag{90}$$

A numerical inspection shows that we can find solutions φ_1, φ_2 of (90) for arbitrary $0 < X_0 < 1$. They define curves in the van der Pauw plane, which start from any point on the upper envelope and go towards the origin $(X,Y) = (0,0)$ with $\chi_1 = 0$. An example is curve 3 in **Figure 9(a)**, which has $X_0 = 0.1$ and $\chi_1 = 0$. Interestingly, in **Figure 9(b)** curve 3 remains at $\mathrm{vdP} \approx 1$ for $0 < r_1 < 0.95$ and only for very large holes $r_1 > 0.95$ the van der Pauw function drops sharply. The numerical computation of curve 3 in **Figure 9(a)** and **Figure 9(b)** is tricky, it needs 5000 digits.

Inserting (21) into (82) into (2) gives the large-hole approximation for star-configurations

$$X^\star \to \exp\left(\frac{(2\varphi_1^\star)^2}{2\ln(r_1)}\right) \quad \text{and} \quad Y^\star \to \exp\left(\frac{(2\varphi_1^\star - \pi)^2}{2\ln(r_1)}\right), \tag{91}$$

which fails if $\varphi_1^\star$ is close to 0 or $\pi/2$. Eliminating $\varphi_1^\star$ in (91) gives the large-hole approximation of the lower envelope,

$$Y^\star \to \exp\left(\frac{\left(\pi - \sqrt{2\ln(r_1)\ln(X^\star)}\right)^2}{2\ln(r_1)}\right), \tag{92}$$

which holds well for $r_1 > 0.45$ and X and Y larger than $\approx \exp\left(\pi^2/(2\ln(r_1))\right)$.

3.8. Checks for Correctness of the Derived Formulae

The formulae of the Section 2 are consistent with [9] for

$$\begin{array}{lll} R_{\text{sheet}} \mapsto \pi\lambda & r_1 \mapsto \exp(-h/2) & \varphi_1 \mapsto (\beta-\alpha)/2 \\ \varphi_1^{\star} \mapsto \phi/2 & \varphi_2 \mapsto \gamma-(\alpha+\beta)/2 & \varphi_3 \mapsto \delta-(\alpha+\beta)/2, \end{array} \tag{93}$$

where the quantities on the left hand sides of (93) are from this article and the quantities on the right hand sides are from [9].

In **Figure 1** the potential ϕ_0 at the outer perimeter for the azimuthal coordinate φ_2 is given by $(-1)\times R_{01,23}$ with $\varphi_3=\pi$, $I_{01}=1$ A. In the limit of vanishing hole size, $r_1\to 0$ it follows from (48) $k=\zeta_4\to 0$ and $K\to\pi/2$. From (52) it follows $F_3=0$. Next we use (57) and (56). With $\mathrm{sn}(u,0)=\sin(u)$ and $\mathrm{dn}(u,0)=1$ and $\mathrm{sc}(u,0)=\tan(u)$ and

$$\Pi(\sin(\omega),n,0)=\frac{\operatorname{artanh}\left(\sqrt{n-1}\tan(\omega)\right)}{\sqrt{n-1}} \tag{94}$$

it follows

$$\phi_0\to\frac{2}{\pi}\operatorname{artanh}\left(\frac{\tan(F_2)}{\tan(F_0)}\right)\to\frac{1}{2\pi}\ln\left(\frac{1-\cos(\varphi_1-\varphi_2)}{1-\cos(\varphi_1+\varphi_2)}\right), \tag{95}$$

which is identical to (A11b) in [17]. Thus, (57) holds in the limit of singly-connected Hall-plates. Moreover, a series expansion of (57) for small k (small r_1) leads to (17). (It is lengthy and arduous and therefore I do not report it in detail here.)

For hole sizes of $r_1=0,0.1,0.5$ and 0.9 I computed the potential in $\varphi_2=15^{\circ},20^{\circ},\cdots,175^{\circ}$ analogous to the preceding paragraph (*i.e.*, via $R_{01,23}$ with $\varphi_3=\pi$) and compared it with results of a finite element simulation with COMSOL Multiphysics. There I used a plane two-dimensional model in application mode "emdc" (static conductive media). Thickness and conductivity were set to 1 m and 1 S/m, respectively. Due to symmetry, only the upper half of the annular ring was modelled with a fine mesh of 917,504 elements. All boundaries were set insulating, except for the segments on the real axis, which were grounded to 0 V. A current of 1 A/m was extracted from contact C_1 at position $\varphi_1=10^{\circ}$. **Figure 10** shows the potential along the perimeter for these four cases and the relative error between analytical and numerical results. The relative errors

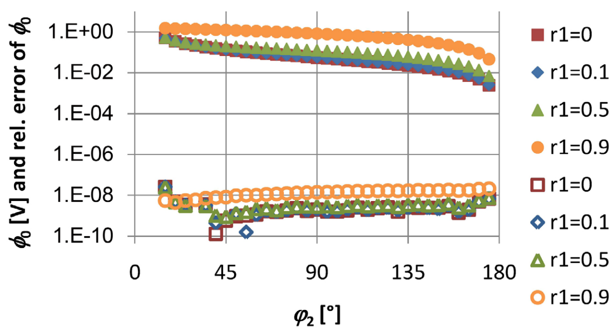

Figure 10. Potential ϕ_0 (full symbols) and relative error of ϕ_0 between analytical formula and FEM-simulation (open symbols) for annular Hall-regions with holes of radius $r_1=0,0.1,0.5,0.9$. The current contacts are at $\varphi_1=10^{\circ}$, and the test points are on the outer perimeter at azimuthal positions φ_2.

are in the order of 10^{-8} which is plausibly due to the finite mesh size around the point-sized current contact. Exemplary numbers for the potential on the unit circle at azimuthal position $\varphi_2 = 25^\circ$ are

$$\begin{aligned} \phi_0 &= 0.2656482094\ \text{V} \quad \text{for } r_1 = 0, \\ \phi_0 &= 0.2666089269\ \text{V} \quad \text{for } r_1 = 0.1, \\ \phi_0 &= 0.3121362860\ \text{V} \quad \text{for } r_1 = 0.5, \\ \phi_0 &= 1.426586599\ \text{V} \quad \text{for } r_1 = 0.9. \end{aligned} \tag{96}$$

As a second numerical check I modelled the Hall-plate in the ζ-plane of Figure 4(c) for the case $r_1 = 0.05$. Equation (36) gives $\zeta_4 = 0.742879765$. Position $\varphi_1 = 80^\circ$ of contacts C_0, C_1 corresponds to $\zeta_0 = 0.612780273$ (see (37)). $\varphi_2 = 130^\circ$ gives $\zeta_2 = -0.3660546310$. $\varphi_3 = 180^\circ$ gives $\zeta_3 = 0$. From (41) it follows $\zeta_5 = 1.283144683$ for the stagnation points in the $R_{01,23}$-case. The finite element model (FEM) uses a handle between $\overline{AB}$ and $\overline{HJ}$ where current flows from Riemann sheet #0 to sheets #1 and # (−1), respectively (see Figure 11). The handle is exactly semi-circular and has anisotropic conductivity $\boldsymbol{\kappa}$ (in radial direction it is zero, and in tangential direction it is $\times 10^6$ bigger than the conductivity of the Hall-plate with $R_{\text{sheet}} = 1\,\Omega$),

$$\kappa_{\xi\xi} = \frac{\kappa_{\text{short}}\eta^2}{\sqrt{\xi^2+\eta^2}}, \quad \kappa_{\eta\eta} = \frac{\kappa_{\text{short}}\xi^2}{\sqrt{\xi^2+\eta^2}}, \quad \kappa_{\xi\eta} = \kappa_{\eta\xi} = \frac{-\kappa_{\text{short}}\xi\eta}{\sqrt{\xi^2+\eta^2}}, \tag{97}$$

whereby $\Re\{\zeta\} = \xi$ and $\Im\{\zeta\} = \eta$. The purpose of the handle is to make a short between points ξ and $-\xi$ for $\zeta_4 \le \xi \le 1$, but not to short any two points inside $\overline{HJ}$.

- In the $R_{01,23}$-case only the right half of the symmetric geometry was modelled with a mesh of 1.8 million elements, see Figure 11(a). A current of $I_{01} = 1\ \text{A}$ was injected into point G and the edges at $\Re\{\zeta\} = 0$ were grounded. According to theory [17], the current through the handle should be $I_{01}(1-\varphi_1/\pi) = 0.5556\ \text{A}$, the FEM result deviates by 486 ppm. The reason might be insufficient meshing and insufficient shorting by the handle (in the FEM, points H and J are not exactly at identical potentials, they are at 68 μV and 8 μV). Point D is at −0.26575 V, which corresponds to $(-1)\times R_{01,23}$, it is 839 ppm larger than the value obtained from (48).
- In the $R_{12,30}$-case the full geometry was modelled with a mesh of 1.1 million elements, see Figure 11(b). A current of 1 A was injected at point C and extracted at point D. Point D was also grounded to 0 V. According to the theory in [17], the current through the handle should be $1\ \text{A}\times(\varphi_2-\varphi_1)/(2\pi) = 0.13889\ \text{A}$, the FEM result deviates by 1120 ppm. Again the handle did not short perfectly: the potential at point B was 2.56193 V, whereas it was 39 μV lower at point H; the potential at point A was 2.48041 V, and it was 2.3 μV lower at point J. The FEM-results for the potentials in point E and G were 2.26454 V and 2.44880 V, respectively. This gives $R_{12,30} = 0.1842613\,\Omega$, which is 462 ppm larger than the result from Formula (48).

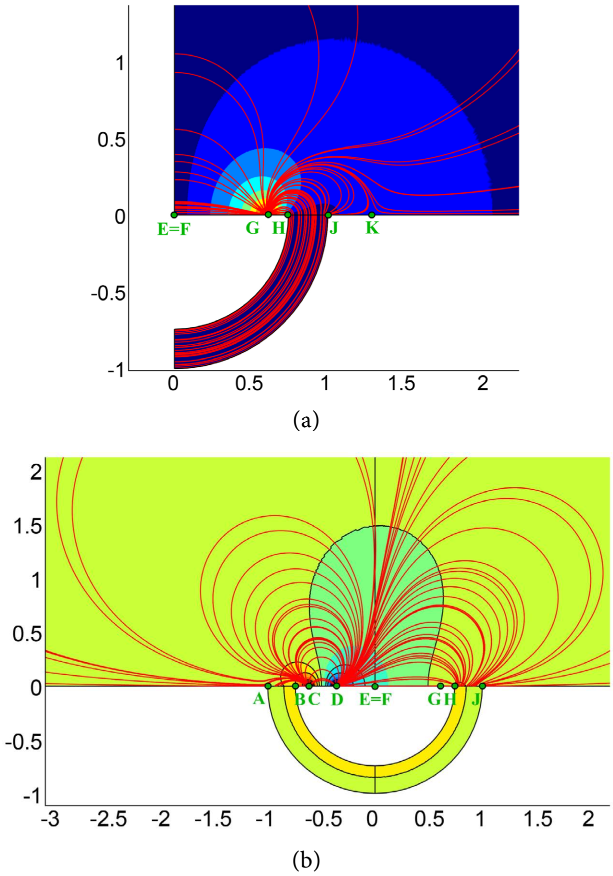

Figure 11. Hall-plate in the ζ -plane with potentials and current streamlines in two operating conditions for $R_{01,23}$ and $R_{12,30}$, respectively. The geometry corresponds to $r_1 = 0.05$, $\varphi_1 = 80^\circ$, $\varphi_2 = 130^\circ$, and $\varphi_3 = 180^\circ$. (a) $R_{01,23}$: Zoom into the region near the short-circuit handle (only the right half is modelled). Vertical edges at left side are grounded. 1 A current is injected into point *G*; (b) $R_{12,30}$: Zoom into the region near the short-circuit handle. 1 A current is injected into *C* and extracted at *D*. *D* is grounded. Current streamlines inside the handle are not drawn.

The analytical formulae give $\text{vdP} = 1 - 5.389 \times 10^{-3}$ and the FEM-simulation gives $\text{vdP} = 1 - 5.543 \times 10^{-3}$. The large vdP-value is due to the small hole, yet for larger holes the point contacts are closer to the handle and the numerical accuracy of the FEM gets even more challenging. This is also a strong indication that in reality the validity of point-sized contacts has to be questioned.

As a by-product of this paper we get a closed form expression of the infinite product

$$\prod_{\ell=1}^{\infty}\left(1-\frac{\cos(\phi)}{\cosh(h\ell)}\right)$$

$$=\frac{1}{\sqrt{2}\sin(\phi/2)}\exp\left(f\left(\frac{3}{4}K,\frac{-K}{4},\frac{K}{4}\right)-f\left(\frac{\pi+\phi}{2\pi}K,\frac{\phi-\pi}{2\pi}K,\frac{\pi-\phi}{2\pi}K\right)\right) \quad (98)$$

with $K = K(k)$, $k = \sqrt{L\left(\frac{h}{2\pi}\right)}$ for $h \ge 0 \wedge 0 \le \phi \le \pi$.

Equation (98) follows from a comparison of the first lines of (27) and (57). It also relates to the prime function of the annular Hall region, see [15].

4. The Hall-Plate at Applied Magnetic Field

As it was shown in [17] the current density does not change when magnetic field is applied, whereas the potential indeed depends on the magnetic field. Thus we can compute the potential at zero magnetic field, ϕ_0, derive its current density $\boldsymbol{J}_0$ and its stream function ψ, and compute the potential $\phi = \phi_0 - \tan(\theta_H)(\psi - \psi_{\text{ground}})$ at arbitrary Hall angle θ_H. Furthermore, in [17] it is derived that the Hall potential is constant along a current streamline (the Hall potential is the difference in electric potential at positive and negative applied magnetic field, it comprises only terms of odd order of the magnetic field). Because of the point-contacts the potential comprises only linear terms of the applied magnetic field, there are no even order terms of the magnetic field (no magneto-resistance terms). Since a current streamline flows from the input contact C_0 to the output contact C_1 along the insulating outer boundary via both voltage contacts C_3, C_2 it follows that the voltage between $C_3 - C_2$ does not depend on the magnetic field. Thus the trans-resistance $R_{01,23}$ does not depend on the applied magnetic field. The same holds for $R_{12,30}$, regardless if there is a hole or not. Therefore, Equations (3) and (4) still hold if magnetic field is applied to the Hall-plate. The situation changes if current flows between the hole boundary and the outer boundary or if there is an extended contact on a boundary, but this goes beyond the scope of this paper.

5. Singly-Connected Hall-Plate with Extended Contacts in Star-Configuration

If a Hall-plate has *no hole* and if its *contacts have finite size* the van der Pauw function also deviates from 1. Thereby the extra degree of freedom from the hole is replaced by the additional parameters for the finite sizes of the contacts. For the simplified case of a star-arrangement of contacts (also called *odd* symmetry in [25]) at zero magnetic field closed analytical formulae are available in the literature (combine [25] with (C24), (C25) in [26]),

$$\begin{gathered}\frac{R_{01,23}}{R_{\text{sheet}}} = \frac{1}{\lambda_1} - \frac{1}{4\lambda_x}, \quad \frac{R_{12,30}}{R_{\text{sheet}}} = \frac{1}{\lambda_2} - \frac{1}{4\lambda_x}, \\ \lambda_1 = \frac{K'\left(\sin(\alpha_1)/\cos(\alpha_2)\right)}{K\left(\sin(\alpha_1)/\cos(\alpha_2)\right)}, \quad \lambda_2 = \frac{K'\left(\sin(\alpha_2)/\cos(\alpha_1)\right)}{K\left(\sin(\alpha_2)/\cos(\alpha_1)\right)}, \\ \frac{1}{4\lambda_x} = \frac{K\left(\sqrt{L(\lambda_1)L(\lambda_2)}\right)}{K'\left(\sqrt{L(\lambda_1)L(\lambda_2)}\right)} = \frac{K\left(\tan(\alpha_1)\tan(\alpha_2)\right)}{K'\left(\tan(\alpha_1)\tan(\alpha_2)\right)},\end{gathered} \tag{99}$$

whereby the angles α_1, α_2 are defined in **Figure 12(a)**. It follows

$$1 \le \text{vdP}_{\text{odd}} = \exp\left(\frac{\pi}{4\lambda_x}\right)\left[\exp\left(\frac{-\pi}{\lambda_1}\right) + \exp\left(\frac{-\pi}{\lambda_2}\right)\right] \le 2, \tag{100}$$

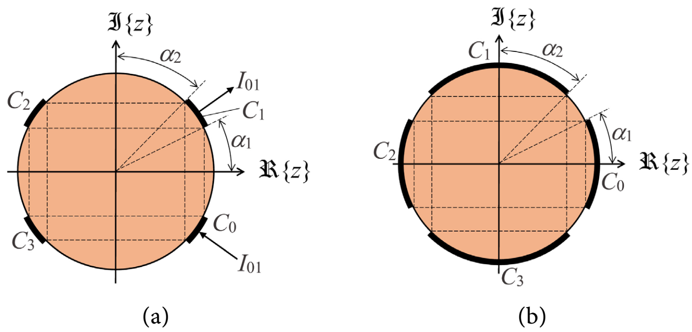

Figure 12. Hall-plates with no hole and with extended symmetric contacts. (a) Star-arrangement of extended contacts (=odd symmetry, [25]); (b) Complementary star-arrangement of extended contacts (=even symmetry, [25]).

for all $\lambda_1 > 0, \lambda_2 > 0$. This is readily proven by plotting vdP versus its two variables λ_1, λ_2 or versus α_1, α_2. The limits are found by the asymptotic limits $K(k \to 0)$ and $K(k \to 1)$. For small contacts $\text{vdP} \to 1$, which is consistent with (3). For large contacts $\text{vdP} \to 2$.

Swapping contacts and isolating boundaries gives the complementary star-configuration (also called *even* symmetry in [25]), see **Figure 12(b)**. There it holds

$$\frac{R_{01,23}}{R_{\text{sheet}}} = \frac{R_{12,30}}{R_{\text{sheet}}} = \frac{\lambda_1 + \lambda_2 - 4\lambda_x}{4},$$
$$\Rightarrow 1 \le \text{vdP}_{\text{even}} = 2\exp\left(-\pi\frac{\lambda_1 + \lambda_2 - 4\lambda_x}{4}\right) \le 2, \tag{101}$$

with $\lambda_1, \lambda_2, \lambda_x$ from (99). λ_1, λ_2 have the following physical meaning: In **Figure 12(b)** the resistance between contacts $C_0 - C_2$, with C_1, C_3 not connected, is equal to $\lambda_1 R_{\text{sheet}}$. The resistance between contacts $C_1 - C_3$, with C_0, C_2 not connected, is equal to $\lambda_2 R_{\text{sheet}}$. Again, for small contacts vdP tends to 1, and for large contacts it tends to 2.

In summary, large contacts increase the van der Pauw function (at least for the symmetric cases of **Figure 12**), whereas a hole reduces it.

6. Conclusions and Suggestions

In this paper, I studied the case of an annular Hall-plate with insulating boundaries and four point-contacts on the perimeter. A conformal transformation $z' = r_1/z$ maps the ring-domain onto itself, thereby swapping inner and outer boundaries. All resistances remain constant under conformal mapping. Hence, upper and lower envelopes also hold if all contacts are on the boundary of the hole.

In practice, one may equip a sample with several point-sized contacts. Four contacts of a first group should be close together, four contacts of a second group should be spaced equidistantly along the full outer boundary. With the first group, one can measure the local sheet resistance via van der Pauw's original method (3). Using this value for the sheet resistance one can use the second group of contacts to determine their respective trans-resistances, from which one can derive vdP with (2). If this value is close to 1 it means that the sample has homogeneous conductivity without hidden holes. If the value obtained for vdP differs markedly from 1, the conductivity is strongly inhomogeneous and there should be at least one hole inside the sample. With **Figure 8** we can assess a lower bound for the size of this hole.

The main results of this article are new proofs of the upper and lower envelopes and closed form expressions for the trans-resistances and the lower envelope in van der Pauw's measurement. This simple geometry of a circular annulus led to a surprisingly complicated Formula (48) for the trans-resistances. Asymptotic limits were derived for small and large holes and specific properties of symmetric contact arrangements were highlighted. The new concepts of contraction and expansion were introduced as well as the small-hole-angle χ_0 and the large-hole-angle χ_1. Yet, several questions are still open for future inquisitions: Is van der Pauw's function vdP monotonously falling with the size of the hole for arbitrary contacts positions? How the general behavior of the trans-resistances versus hole size is? What happens, if not all contacts are on the same boundary? Is there a qualitative difference for contacts of finite size? What happens if the hole boundary is conducting such that the hole is short instead of a void? And finally, what happens if the Hall-plate has more than one hole?

Acknowledgements

Sincere thanks to Michael Holliber for his help in **Figure 5(a)**.

Conflicts of Interest

The author declares no conflicts of interest regarding the publication of this paper.

References

[1] van der Pauw, L.J. (1958) A Method of Measuring Specific Resistivity and Hall Effect of Discs of Arbitrary Shape. *Philips Research Reports*, **13**, 1-9.

[2] van der Pauw, L.J. (1958) A Method of Measuring Specific Resistivity and Hall Coefficient on Lamellae of Arbitrary Shape. *Philips Technical Review*, **20**, 220-224.

[3] Wasscher, J.D. (1961) Note on Four-Point Resistivity Measurements on Anisotropic Conductors. *Philips Research Reports*, **16**, 301-306.

[4] van der Pauw, L.J. (1961) Determination of Resistivity Tensor and Hall Tensor of Anisotropic Conductors. *Philips Research Reports*, **16**, 187-195.

[5] Ausserlechner, U. (2018) An Analytical Theory of Piezoresistive Effects in Hall Plates with Large Contacts. *Advances in Condensed Matter Physics*, **2018**, Article ID: 7812743. https://doi.org/10.1155/2018/7812743

[6] Bierwagen, O., Ive, T., Van de Walle, C.G. and Speck, J.S. (2008) Causes of Incorrect Carrier-Type Identification in van der Pauw-Hall Measurements. *Applied Physics Letters*, **93**, Article ID: 242108. https://doi.org/10.1063/1.3052930

[7] Náhlík, J., Kašpárková, I. and Fitl, P. (2011) Study of Quantitative Influence of Sample Defects on Measurements of Resistivity of Thin Films Using van der Pauw Method. *Measurement*, **44**, 1968-1979.

https://doi.org/10.1016/j.measurement.2011.08.023

[8] Koon, D.W., Wang, F., Petersen, D.H. and Hansen, O. (2014) Sensitivity of Resistive and Hall Measurements to Local Inhomogeneities: Finite-Field, Intensity, and Area Corrections. *Journal of Applied Physics*, **116**, Article ID: 133706. https://doi.org/10.1063/1.4896947

[9] Szymański, K., Cieśliński, J.L. and Łapiński, K. (2013) Van der Pauw Method on a Sample with an Isolated Hole. *Physics Letters A*, **377**, 651-654. https://doi.org/10.1016/j.physleta.2013.01.008

[10] Szymański, K., Łapiński, K. and Cieśliński, J.L. (2013) Determination of a Geometrical Parameter by the van der Pauw Method. https://www.semanticscholar.org/paper/Determination-of-a-geometrical-parameter-by-the-van-Szyma%C5%84ski-%C5%81api%C5%84ski/fb494fd99c53788a7bf1a73fe1041dc26cca3f68 https://arxiv.org/abs/1412.0707v1?msclkid=3630a53aad0911ec9bb13a222b9cce60

[11] Szymański, K., Łapiński, K., Cieśliński, J.L., Kobus, A., Zaleski, P., Biernacka, M., *et al.* (2015) Determination of the Riemann Modulus and Sheet Resistivity by a Six-Point Generalization of the van der Pauw Method. *Measurement Science and Technology*, **26**, Article ID: 085012. https://doi.org/10.1088/0957-0233/26/8/085012

[12] Szymański, K.R., Walczyk, C.J. and Cieśliński, J.L. (2019) Determination of Topological Properties of Thin Samples by the van der Pauw Method. *Measurement*, **145**, 568-572. https://doi.org/10.1016/j.measurement.2019.05.075

[13] Oh, D., Ahn, C., Kim, M., Park, E-K. and Kim, Y-S. (2016) Application of the van der Pauw Method for Samples with Holes. *Measurement Sciences and Technology*, **27**, Article ID: 125001. https://doi.org/10.1088/0957-0233/27/12/125001

[14] Miyoshi, H., Crowdy, D.G. and Nelson, R. (2021) Fay Meets van der Pauw: The Trisecant Identity and the Resistivity of Holey Samples. *Proceedings of the Royal Society A*, **477**, Article ID: 20200796. https://doi.org/10.1098/rspa.2020.0796

[15] Miyoshi, H., Crowdy, D.G. and Nelson, R. (2021) The Prime Function, the Fay Trisecant Identity, and the van der Pauw Method. *Computational Methods and Function Theory*, **21**, 707-736. https://doi.org/10.1007/s40315-021-00409-1

[16] Mani, R.G. and von Klitzing, K. (1994) Temperature-Insensitive Offset Reduction in a Hall Effect Device. *Applied Physics Letters*, **64**, 3121-3123. https://doi.org/10.1063/1.111974

[17] Ausserlechner, U. (2019) The Classical Hall Effect in Multiply-Connected Plane Regions Part I: Topologies with Stream Function. *Journal of Applied Mathematics and Physics*, **7**, 1968-1996. https://doi.org/10.4236/jamp.2019.79136

[18] Goluzin, G.M. (1969) Geometric Function Theory of a Complex Variable. Vol. 26, American Mathematical Society, Providence.

[19] Prudnikov, A.P., Brychkov, Yu., A. and Marichev, O.I. (1986) Integrals and Series, 1.2.62.3. Vol. 1, Gordon and Breach Science Publishers S.A., New York.

[20] Sample, H.H., Bruno, W.J., Sample, S.B. and Sichel, E.K. (1987) Reverse-Field Reciprocity for Conducting Specimens in Magnetic Fields. *Journal of Applied Physics*, **61**, 1079-1084. https://doi.org/10.1063/1.338202

[21] https://functions.wolfram.com/EllipticIntegrals/EllipticPi/27/01/0001/

[22] https://functions.wolfram.com/EllipticIntegrals/EllipticPi3/17/01/0002/

[23] https://functions.wolfram.com/EllipticIntegrals/EllipticPi3/17/01/0004/

[24] https://functions.wolfram.com/EllipticIntegrals/JacobiZeta/16/02/01/0002/

[25] Ausserlechner, U. (2017) Van-der-Pauw Measurement on Devices with Four Contacts and Two Orthogonal Mirror Symmetries. *Solid-State Electronics*, **133**, 53-63. https://doi.org/10.1016/j.sse.2017.04.006

[26] Ausserlechner, U. (2018) An Analytical Theory of the Signal-to-Noise Ratio of Hall Plates with Four Contacts and a Single Mirror Symmetry. *Journal of Applied Mathematics and Physics*, **6**, 2032-2066. https://doi.org/10.4236/jamp.2018.610174

[27] Nehari, Z. (1952) Mapping Properties of Special Functions. In: *Conformal Mapping*, Dover Publications, Inc., New York.

[28] https://functions.wolfram.com/EllipticIntegrals/EllipticF/16/02/01/0001/

[29] https://functions.wolfram.com/EllipticIntegrals/EllipticE2/16/02/01/0001/

[30] https://functions.wolfram.com/EllipticFunctions/JacobiSN/16/02/0001/

Appendix A

The geometric series is

$$\sum_{\ell=0}^{\infty} q^{\ell} = \frac{1}{1-q} \quad \text{for } |q| \le 1 \wedge q \ne 1. \tag{102}$$

With (102) it follows

$$\begin{aligned}\sum_{\ell=0}^{\infty} r^{\ell} \cos\left(\alpha(\ell+1)\right) &= \frac{1}{2r}\sum_{\ell=0}^{\infty}\left(r\exp(i\alpha)\right)^{\ell+1} + \left(r\exp(-i\alpha)\right)^{\ell+1} \\ &= \frac{1}{2r}\left(\sum_{m=0}^{\infty}\left[\left(r\exp(i\alpha)\right)^{m} + \left(r\exp(-i\alpha)\right)^{m}\right] - 2\right) \\ &= \frac{1}{2r}\left(\frac{1}{1-r\exp(i\alpha)} + \frac{1}{1-r\exp(-i\alpha)} - 2\right) \\ &= \frac{\cos(\alpha) - r}{1+r^2-2r\cos(\alpha)},\end{aligned} \tag{103}$$

whereby $|r| < 1 \wedge \alpha \in \mathbb{R}$ or $|r| = 1 \wedge \alpha \ne 2\pi\ell, \ell \in \mathbb{Z}$. We can integrate the very left and right sides of (103), whereby the series on the left side can be integrated term-wise, because integration improves the convergence. This gives

$$\begin{aligned}\sum_{\ell=0}^{\infty} \frac{x^{\ell+1}}{\ell+1}\cos\left(\alpha(\ell+1)\right) &= \int_{r=0}^{x} \frac{\cos(\alpha)-r}{1+r^2-2r\cos(\alpha)}\mathrm{d}r \\ \Rightarrow \sum_{m=1}^{\infty}\frac{x^m}{m}\cos(m\alpha) &= \frac{-1}{2}\ln\left(1+x^2-2x\cos(\alpha)\right),\end{aligned} \tag{104}$$

for $|x| < 1 \wedge \alpha \in \mathbb{R}$ or $|x| = 1 \wedge \alpha \ne 2\pi\ell, \ell \in \mathbb{Z}$. With (104) it holds

$$\begin{aligned}&\sum_{m=1}^{\infty}\frac{x^m}{m}\sin(m\alpha)\sin(m\beta) \\ &= \sum_{m=1}^{\infty}\frac{x^m}{2m}\left(\cos\left((\alpha-\beta)m\right) - \cos\left((\alpha+\beta)m\right)\right) \\ &= \frac{1}{4}\ln\left(\frac{1+x^2-2x\cos(\alpha+\beta)}{1+x^2-2x\cos(\alpha-\beta)}\right),\end{aligned} \tag{105}$$

for $|x| < 1 \wedge (\alpha,\beta) \in \mathbb{R}^2$ or $|x| = 1 \wedge \alpha \pm \beta \ne 2\pi\ell, \ell \in \mathbb{Z}$.

Appendix B

Definition of the incomplete elliptic integral of the first kind

$$F(u,k) = \int_0^u \frac{\mathrm{d}x}{\sqrt{1-x^2}\sqrt{1-k^2x^2}} = \int_0^{\arcsin(u)} \frac{\mathrm{d}\alpha}{\sqrt{1-k^2\sin^2\alpha}} \tag{106}$$

with $-1 \le u \le 1 \wedge -1 \le k \le 1$. $\text{EllipticF}\left[\text{ArcSin}[u], k^2\right]$ is the Mathematica notation of $F(u,k)$. This function is strictly monotonic in *u* and *k*. The complete elliptic integral of the first kind is $K(k) = F(1,k)$. Its Mathematica notation is $\text{EllipticK}\left[k^2\right]$. The complementary elliptic integral of the first kind is denoted by a prime $K'(k) = K\left(\sqrt{1-k^2}\right)$. For $1 \le u \le 1/k$ Equation (106) gives

$$\int_1^u \frac{\mathrm{d}x}{\sqrt{x^2-1}\sqrt{1-k^2x^2}} = K'(k) - F\left(\sqrt{\frac{1-k^2u^2}{1-k^2}}, \sqrt{1-k^2}\right). \tag{107}$$

For $u = 1/k$ this gives

$$K'(k) = \int_1^{1/k} \frac{\mathrm{d}x}{\sqrt{x^2-1}\sqrt{1-k^2x^2}}. \tag{108}$$

The incomplete elliptic integral of the second kind is

$$E(u,k) = \int_0^u \frac{\sqrt{1-k^2x^2}}{\sqrt{1-x^2}}\mathrm{d}x = \int_0^{\arcsin u} \sqrt{1-k^2\sin^2\alpha}\,\mathrm{d}\alpha, \tag{109}$$

with $-1 \le u \le 1 \wedge -1 \le k \le 1 \wedge k \ne 0$. The complete elliptic integral of the second kind is $E(k) = E(1,k)$. The Mathematica notations of $E(u,k)$ and $E(k)$ are $\text{EllipticE}\left[\text{ArcSin}[u], k^2\right]$ and $\text{EllipticE}\left[k^2\right]$, respectively. Definition of the incomplete elliptic integral of the third kind

$$\begin{aligned}\Pi(u,n,k) &= \int_0^u \frac{\mathrm{d}x}{\left(1-nx^2\right)\sqrt{1-x^2}\sqrt{1-k^2x^2}} \\ &= \int_0^{\arcsin(u)} \frac{\mathrm{d}\alpha}{\left(1-n\sin^2\alpha\right)\sqrt{1-k^2\sin^2\alpha}}\end{aligned} \tag{110}$$

with $-1 \le u \le 1 \wedge -1 \le k \le 1$ with $n < 1/u^2$. The complete elliptic integral of the third kind is $\Pi(n,k) = \Pi(1,n,k)$. $\text{EllipticPi}\left[n, \text{ArcSin}[u], k^2\right]$ and $\text{EllipticPi}\left[n, k^2\right]$ are the Mathematica notations of $\Pi(u,n,k)$ and $\Pi(n,k)$, respectively. The Jacobi-zeta function is

$$Z(u,k) = E(u,k) - \frac{E(k)}{K(k)}F(u,k), \tag{111}$$

with the Mathematica notation $\text{JacobiZeta}\left[\text{ArcSin}[u], k^2\right]$. Frequently we are interested in aspect ratios of rectangles from conformal maps of Hall-plates. Then the ratio $y = K'(k)/K(k)$ shows up. This function is monotonic. Thus, its inverse exists, this is the modular lambda elliptic function $L(y)$ [27].

$$L\left(\frac{K'(k)}{K(k)}\right) = k^2 \quad \text{for } -1 \le k \le 1 \tag{112}$$

The Mathematica notation is $\text{ModularLambda}[iy] = L(y)$. Several properties of $L(y)$ are explained in [25].

Inversion of (106) gives the Jacobi-sn function and the Jacobi amplitude

$$u = \text{sn}(F(u,k),k) \quad \text{and} \quad \arcsin(u) = \text{am}(F(u,k),k). \tag{113}$$

The Mathematica notation is $\text{JacobiSN}\left[u,k^2\right] = \text{sn}(u,k)$. Thus it holds $\text{sn}(u,k) = \sin(\text{am}(u,k))$ with further Jacobi functions like $\text{cn}(u,k) = \cos(\text{am}(u,k))$ and $\text{dn}(u,k) = \sqrt{1-k^2\text{sn}^2(u,k)}$. Like $F(u,k)$ also $\text{sn}(u,k)$ is odd in u and even in k and strictly monotonic in u and k as long as

$-K(k) \le u \le K(k)$ and $-1 \le k \le 1$. It follows

$$\mathrm{sn}(0,k)=0 \quad \text{and} \quad \mathrm{sn}(\pm K(k),k)=\pm 1. \tag{114}$$

Yet, for $u > K(k)$ the Jacobi-sn function has a real-valued period $4K(k)$ and a half-period $2K(k)$.

$$\mathrm{sn}(u+2K(k),k)=-\mathrm{sn}(u,k) \quad \text{and} \quad \mathrm{sn}(u+4K(k),k)=\mathrm{sn}(u,k). \tag{115}$$

It holds

$$\begin{aligned} &\mathrm{sn}(u,0)=\sin(u), \quad F(u,0)=\arcsin(u), \\ &\Pi(u,0,k)=F(u,k), \quad Z(u,0)=0. \end{aligned} \tag{116}$$

It also holds

$$\begin{aligned} &K(k\to 1)=\ln\left(\frac{4}{\sqrt{1-k^2}}\right), \quad E(1)=1, \\ &\mathrm{sn}(u,1)=\tanh(u), \quad E(u,1)=u, \\ &\Pi(u,n,1)=\frac{1}{2(n-1)}\left\{\ln\left(\frac{1-u}{1+u}\right)+\sqrt{n}\ln\left(\frac{1-u\sqrt{n}}{1+u\sqrt{n}}\right)\right\}, \end{aligned} \tag{117}$$

for $-1<u<1$ and $0<n<1/u^2$. From (111), (117), and (113) it follows

$$Z(\mathrm{sn}(u,1),1)=E(\mathrm{sn}(u,1),1)-\frac{E(1)}{K(k\to 1)}u=\tanh(u). \tag{118}$$

Appendix C

An alternative proof of (66) is by direct computation of the partial derivatives $f^{(1,0,0)}, f^{(0,1,0)}$. Thereby $f^{(1,0,0)}$ is a long expression, which is most conveniently computed with an algebraic program like e.g. Mathematica. It comprizes elliptic-Pi functions, $\Pi(\mathrm{sn}(x_0-K),\mathrm{sn}^{-2}(x_0),k)$ and $\Pi(1-\mathrm{dn}^2(x_0),k)$, which are multiplied by terms that can be shown to vanish. There is also a term $\mathrm{dn}^2(x_0)$, which is multiplied by $K(k)-x_0+F(\mathrm{sn}(x_0-K(k)),k)$, which also vanishes, since F is the inverse function of sn. The remainder is

$$\begin{aligned} &f^{(1,0,0)}(x_0,x_0-K,K-x_0) \\ &=2\left\{E(k)\left(\frac{x_0}{K(k)}-1\right)-E(\mathrm{sn}(x_0-K(k)),k)+\frac{k^2(1-k^2)\mathrm{cn}(x_0)\mathrm{sn}(x_0)}{\mathrm{dn}(x_0)(k^2-1+\mathrm{dn}^4(x_0))}\right\}. \end{aligned} \tag{119}$$

$E(z,k)$ and $E(k)$ are incomplete and complete elliptic integrals of the second kind (see Appendix B). For the other partial derivative one gets

$$\begin{aligned} &f^{(0,1,0)}(x_0,x_0-K,K-x_0) \\ &=\frac{\mathrm{dn}(x_0)}{\mathrm{sc}(x_0)}\left(\frac{k^2-1+\mathrm{dn}^2(x_0)}{k^2-1+\mathrm{dn}^4(x_0)}-\frac{\Pi(1-\mathrm{dn}^2(x_0),k)}{K(k)}\right). \end{aligned} \tag{120}$$

We use the following identities

$$\begin{aligned}
&\Pi\left(1-\mathrm{dn}^2\left(x_0\right),k\right)\\
&=K\left(k\right)+\frac{\mathrm{sc}\left(x_0\right)}{\mathrm{dn}\left(x_0\right)}\left(K\left(k\right)E\left(\mathrm{sn}\left(x_0\right),k\right)-E\left(k\right)F\left(\mathrm{sn}\left(x_0\right),k\right)\right),\\
&F\left(\mathrm{sn}\left(x_0-K\left(k\right)\right),k\right)=F\left(\mathrm{sn}\left(x_0\right),k\right)-K\left(k\right),\\
&E\left(\mathrm{sn}\left(x_0-K\left(k\right)\right),k\right)=E\left(\mathrm{sn}\left(x_0\right),k\right)-E\left(k\right)-k^2\frac{\mathrm{cn}\left(x_0\right)\mathrm{sn}\left(x_0\right)}{\mathrm{dn}\left(x_0\right)}.
\end{aligned} \tag{121}$$

The first equation can be found in [21]. The other two equations follow from the addition formulas for elliptic F- and E-functions [28] [29], and for the Jacobi-sn function [30]. Equations (121) are at least valid in $0 \le x_0 < K$. Finally we subtract twice (120) from (119) and insert (121). Then all terms cancel out, which completes the proof of (66).

Appendix D

Table A1. Notation list of all the variables of this work.

$C_0,\cdots,C_3$	contacts of the Hall-plate
$f\left(x,y,z\right)$	special function expresses the trans-resistances of the Hall-plate
r_1	radius of the hole in the unit disk
$R_{k\ell,mn}$	trans-resistances of the Hall-plate
R_{sheet}	sheet resistance of the Hall-plate
vdP	van der Pauw function
X,Y	coordinates in the van der Pauw plane
X_0,Y_0	X,Y for Hall-plates without a hole
X_1,Y_1	X,Y for Hall-plates in the limit of a very large hole
χ_0,χ_1	angles in the van der Pauw plane
ϕ_0	electric potential at zero magnetic field
$\varphi_1,\cdots,\varphi_3$	general azimuthal coordinates of the contacts
$\kappa_{\xi,\eta}$	Cartesian components of the conductivity tensor in the ζ -plane
ϑ	exponent used in the large hole approximation
$\zeta_0,\cdots,\zeta_5$	specific locations in the ζ -plane
$\star$	denotes parameters for a star-configuration of the contacts
K,E,Π,K',E'	elliptic integrals and complementary ones

Continued

Z	Jacobi-zeta function
L	modular lambda elliptic function
$\mathrm{am}, \mathrm{sn}, \mathrm{cn}, \mathrm{dn}, \mathrm{sc}$	Jacobi functions